

# Chemical abundances of magnetic and non-magnetic Herbig Ae/Be stars

C.P. Folsom<sup>1\*</sup>, S. Bagnulo<sup>1</sup>, G.A. Wade<sup>2</sup>, E. Alecian<sup>3</sup>, J.D. Landstreet<sup>1,4</sup>,  
S.C. Marsden<sup>5,6</sup>, I.A. Waite<sup>7</sup>

<sup>1</sup>*Armagh Observatory, College Hill, Armagh Northern Ireland BT61 9DG*

<sup>2</sup>*Department of Physics, Royal Military College of Canada, P.O. Box 17000, Station ‘Forces’, Kingston, Ontario, Canada, K7K 7B4*

<sup>3</sup>*Observatoire de Paris, LESIA, Place Jules Janssen, F-92195 Meudon Cedex, France*

<sup>4</sup>*Physics & Astronomy Department, The University of Western Ontario, London, Ontario, Canada, N6A 3K7*

<sup>5</sup>*Australian Astronomical Observatory, PO Box 296, Epping, Sydney, 1710, Australia*

<sup>6</sup>*Centre for Astronomy, School of Engineering and Physical Sciences, James Cook University, Townsville, 4811, Australia*

<sup>7</sup>*Faculty of Sciences, University of Southern Queensland, Toowoomba, 4350, Australia*

Received: 201?; Accepted: 201?

## ABSTRACT

The photospheres of about 10-20% of main sequence A- and B-type stars exhibit a wide range of chemical peculiarities, often associated with the presence of a magnetic field. It is not exactly known at which stage of stellar evolution these chemical peculiarities develop. To investigate this issue, in this paper we study the photospheric compositions of a sample of Herbig Ae and Be stars, which are considered to be the pre-main sequence progenitors of A and B stars. We have performed a detailed abundance analysis of 20 Herbig stars (three of which have confirmed magnetic fields), and one dusty young star. We have found that half the stars in our sample show  $\lambda$  Boo chemical peculiarities to varying degrees, only one star shows weak Ap/Bp peculiarities, and all the remaining stars are chemically normal. The incidence of  $\lambda$  Boo chemical peculiarities we find in Herbig stars is much higher than what is seen on the main sequence. We argue that a selective accretion model for  $\lambda$  Boo star formation is a natural explanation for the remarkably large number of  $\lambda$  Boo stars in our sample. We also find that the magnetic Herbig stars do not exhibit a range of chemical compositions remarkably different from the normal stars: one magnetic star displays  $\lambda$  Boo chemical peculiarities (HD 101412), one displays weak Ap/Bp peculiarities (V380 Ori A), and one (HD 190073) is chemically normal. This is completely different from what is seen on the main sequence, where all magnetic A and cool B stars show Ap/Bp chemical peculiarities, and this is consistent with the idea that the magnetic field precedes the formation of the chemical peculiarities typical of Ap and Bp stars.

**Key words:** stars: magnetic fields, stars: abundances, stars: chemically peculiar, stars: pre-main-sequence

## 1 INTRODUCTION

In main sequence A and B stars a wide range of peculiar chemical abundances are observed. While much study has been devoted to these peculiar objects, a lot remains to be learnt about the physical processes behind these chemical peculiarities. An avenue of study that has not yet been properly investigated is to examine the chemistry in the pre-main sequence progenitors of main sequence peculiar stars.

Herbig Ae and Be (HAeBe) stars are pre-main sequence A and B stars, and thus evolve into the wide range of dif-

ferent main sequence A and B stars. Observationally, Herbig stars are generally identified by optical emission lines, infrared excess, and are usually associated with nebulous regions (Vieira et al. 2003). Chemically, these stars are thought to possess approximately solar abundances (Acke & Waelkens 2004), similar to most young, nearby main sequence stars.

A small number of HAeBe stars have recently been found to have strong, globally ordered magnetic fields (Donati et al. 1997; Wade et al. 2005, 2007; Catala et al. 2007; Alecian et al. 2008a,b). The strength and morphology of these magnetic fields are very similar to those seen in the magnetic chemically peculiar Ap and Bp stars (Alecian et al.

\* E-mail: cpf@arm.ac.uk

2008a; Folsom et al. 2008; Alecian et al. 2009), making these magnetic HAeBe stars strong candidates for the progenitors of Ap and Bp stars (Wade et al. 2005). This discovery in particular raises the question of whether any sign of chemical peculiarity can be found on the pre-main sequence.

In main sequence A and cooler B stars, magnetic fields are always seen together with the characteristic chemical peculiarities of Ap and Bp stars (Aurière et al. 2007). Hotter magnetic B stars also usually show chemical peculiarities, such as He-weak or He-strong stars. Consequently, if magnetic HAeBe stars evolve into Ap and Bp stars, then at some point they must develop chemical peculiarities. Detecting such peculiarities on the pre-main sequence would provide new constraints on the timescales on which, and the conditions under which, these peculiarities evolve.

A few detections of chemical peculiarities in very young stars near or on the zero-age main sequence provide tantalising hints that chemical peculiarities may be common in magnetic Herbig Ae/Be stars. Some notable cases of this are V380 Ori (Alecian et al. 2009), HD 72106 A (Folsom et al. 2008), NGC 6611 W601 (Alecian et al. 2008b), and perhaps NGC 2244-334 (Bagnulo et al. 2004) which is a very young main sequence star. Recent modelling by Vick et al. (2011) of chemical diffusion in the presence of modest mass loss suggest it is possible for chemical peculiarities to form during the pre-main sequence phase. Interestingly, Cowley et al. (2010) found a different form of chemical peculiarities,  $\lambda$  Boötis peculiarities, in the Herbig Ae star HD 101412.

$\lambda$  Boötis stars are mostly main sequence A stars, with strong underabundances of many metals, particularly iron peak elements. Lighter elements, specifically C, N, O, S, and in some cases Na, have normal abundances, while iron peak elements are usually depleted by  $\sim 1$  dex (e.g. Venn & Lambert 1990; Andrievsky et al. 2002; Heiter 2002). This is in contrast to almost all other chemically peculiar A and B stars, which are characterised by strong overabundances of iron peak elements.  $\lambda$  Boo stars have not been found to have magnetic fields, unlike Ap and Bp stars (Bohlender & Landstreet 1990).  $\lambda$  Boo stars have a distribution of  $v \sin i$  values that is the same as for normal A and B stars (e.g. Abt & Morrell 1995), unlike Ap or Am stars.

The cause of the peculiar abundances seen in  $\lambda$  Boo stars remains unknown, though a number of hypotheses have been suggested. The most popular hypothesis is that the peculiarities are a result of a selective accretion process (Venn & Lambert 1990; Waters et al. 1992). In this scenario, gas depleted in heavier elements is accreted preferentially, building up a layer of relative underabundance in heavier elements at the surface of the star. A proposed mechanism for this suggests that heavier elements are bound into dust grains, which are then preferentially driven away from the star by its radiation, while gas, which is depleted in heavier elements as a consequence of dust formation, is more readily accreted (e.g. Andrievsky & Paunzen 2000). Thus, because of the lack of significant convective mixing in the atmospheres of A-type stars, a layer that is underabundant in heavier elements is quickly built up at the surface of the star.

A variation on this hypothesis is that the  $\lambda$  Boo peculiarities result from selective accretion of gas in the interstellar medium, rather than pre-existing circumstellar material (Kamp & Paunzen 2002). In this scenario the star passes through a diffuse interstellar cloud, in which heavier

elements are already preferentially bound into dust grains. The star then accretes the metal poor gas, while driving away the dust by radiation pressure.

Other hypotheses have been put forward to explore the origins of  $\lambda$  Boo stars. For example it has been suggested that  $\lambda$  Boo stars are actually spectroscopic binaries (Faragiana & Bonifacio 2005), thus the apparent under abundances would be due to continuum emission from a secondary, but this hypothesis is largely discounted (Stütz & Paunzen 2006). Radiatively driven atomic diffusion, which is the most widely accepted mechanism for forming peculiarities in most chemically peculiar A and B stars, has been considered for  $\lambda$  Boo stars with the addition of mass loss (Michaud & Charland 1986). However, any turbulent or rotational mixing impedes the process sufficiently to prevent it from forming  $\lambda$  Boo peculiarities (Charbonneau 1993). Since  $\lambda$  Boo stars rotate with similar  $v \sin i$  to normal A stars, they potentially can have significant rotational mixing. Thus atomic diffusion is generally considered to be insufficient to cause  $\lambda$  Boo peculiarities.

Numerical models of  $\lambda$  Boo star atmospheres including the accretion of material depleted in heavier elements, together with atomic diffusion, have been made by Turcotte & Charbonneau (1993) and Turcotte (2002). They find that those models can produce  $\lambda$  Boo peculiarities quickly ( $\sim 0.1$  Myr) for gas accretion rates of  $\sim 10^{-13} M_{\odot} \text{ yr}^{-1}$ , but the peculiarities in these models do not last long after accretion has stopped ( $\sim 1$  Myr). The peculiarities in these models appear to persist despite rotational mixing (Turcotte & Charbonneau 1993), but larger surface convection zones require larger accretion rates to produce the same peculiarities (Turcotte 2002).

In order to help address the question of  $\lambda$  Boo star formation, and to investigate when Ap/Bp stars develop chemical peculiarities, we have analysed high resolution spectra of 20 Herbig Ae/Be stars, and one dusty young star. We have determined atmospheric parameters and performed a detailed abundance analysis for these stars, with the goal of detecting chemical peculiarities. Three of these stars have confirmed magnetic field detections, and thus may be the progenitors of Ap/Bp stars. The other 18 stars have been carefully searched for magnetic fields, but no confirmed magnetic fields have been found.

## 2 OBSERVATIONS

Observations for this study were obtained with the Echelle Spectropolarimetric Device for the Observation of Stars (ESPaDONs) instrument at the Canada France Hawaii Telescope (CFHT). ESPaDONs is a high-resolution échelle spectropolarimeter, providing nearly continuous wavelength coverage from 3700 to 10500 Å at a resolution of  $R = 65000$ . All observations were obtained in spectropolarimetric mode, which provides circularly polarised Stokes  $V$  spectra, as well as total intensity Stokes  $I$  spectra. Data reduction was performed with the Libre-ESPRIT (Donati et al. 1997) package, which is optimised for the ESPaDONs instrument, and performs calibrations and optimal spectrum extraction.

The observations were obtained over several years, between 2004 and 2006 as part of an extended campaign investigating the presence of magnetic fields in Herbig Ae and

Be stars. This study is discussed as a whole by Alecian et al. (2012a), and individual results are reported by Wade et al. (2005), Catala et al. (2007), Alecian et al. (2008a), Alecian et al. (2008b), Folsom et al. (2008), and Alecian et al. (2009). The observations that were analysed for this paper are reported in Table 1. Additional observations from Alecian et al. (2012a) were used to check for variability in spectral lines. The high resolution and high S/N necessary for the detection of magnetic fields in metallic lines also makes these observations very well suited to a detailed abundance analysis, thus we have an excellent dataset for our study.

The stars analysed in this study are only a subset of the full set of targets observed by Alecian et al. (2012a). The stars selected for our study were chosen to cover a range of  $T_{\text{eff}}$  and  $v \sin i$  values. The stars were also selected to generally have only modest amounts of emission in their optical spectra, which allows for a more complete and accurate abundance analysis. Preference was given to stars that were not clearly spectroscopic binaries, and to observations with a peak S/N over 200. Stars with a confirmed magnetic field and a  $T_{\text{eff}}$  below 15000 K were all included (except for HD 72106 A, which was studied in detail by Folsom et al. 2008).

Observations of one star (HD 101412) were obtained from the Anglo-Australian Telescope (AAT) with the University College London Echelle Spectrograph (UCLES) together with SEMPOL polarimeter. This instrument consists of a bench mounted cross-dispersed échelle spectrograph (UCLES) fibre fed from a Cassegrain mounted polarimeter unit (SEMPOL), and is fundamentally a similar instrument to ESPaDOnS. Details of the instrument can be found in Semel et al. (1993) and Donati et al. (1997, 2003), and the observing run that the observations of HD 101412 were obtained in is described by Marsden et al. (2011). Data reduction and optimal spectral extraction were performed with a generic version of ESPRIT (Donati et al. 1997).

Supplemental archival observations from the FORS1 instrument at the Very Large Telescope (VLT) were used for examining Balmer lines in many stars, and are listed in Table 2. FORS1 is a low resolution spectropolarimeter, which produces an observed spectrum entirely in one order. This is useful as it reduces the possibility of normalisation errors across Balmer lines. The observations were obtained from the study of Wade et al. (2007), and a detailed description of the observations and data reduction techniques can be found therein. While Wade et al. (2007) focused on detecting magnetic fields, we only concern ourselves with Balmer line profile shapes.

### 3 FUNDAMENTAL PARAMETERS

Temperature and surface gravity were first measured by fitting Balmer lines, and then confirmed and, if possible, refined by enforcing local thermodynamic equilibrium (LTE) ionisation and excitation balances in the metallic line spectra of the stars during the modelling procedure.

Balmer line fitting was performed on FORS1 spectra when available, since it is easier to normalise broad spectral features when they are recorded entirely in one spectral order. When FORS1 spectra were not available, ESPaDOnS spectra were used and careful attention was paid to the normalisation of Balmer lines. Continuum points well

**Table 1.** Table of observations for which an abundance analysis was performed. The Heliocentric Julian date, total integration time, and peak signal-to-noise ratio (per  $1.8 \text{ km s}^{-1}$  spectral pixel) in Stokes  $I$  are presented for each observation.

Object	HJD	Integration Time (s)	Peak S/N $I$
HD 17081	2453422.7286	480	878
HD 31293	2453423.8512	2400	471
HD 31648	2453423.8840	2400	334
HD 36112	2453421.7718	2400	239
HD 68695	2453423.9585	2400	112
HD 139614	2453422.0790	3600	222
HD 141569	2454167.0581	5400	877
HD 142666	2453424.0544	3600	288
HD 144432	2453423.1169	3200	312
HD 163296	2453607.7370	1200	538
HD 169142	2453606.8006	2000	394
HD 176386	2453607.7587	1600	479
HD 179218	2453608.8447	1600	532
HD 244604	2453607.0733	3600	276
HD 245185	2453421.8207	4800	146
HD 278937	2453422.7664	4800	167
T Ori	2453607.1183	3600	204
HD 101412	2454194.9520	7200	150
HD 190073	2454167.1543	2700	496
V380 Ori	2453609.0940	4800	256

**Table 2.** FORS1 observations used for Balmer line fitting, obtained by Wade et al. (2007). The Heliocentric Julian date, total integration time, and peak signal-to-noise ratio (per  $64 \text{ km s}^{-1}$  spectral pixel) in Stokes  $I$  are presented for each observation.

Object	HJD	Integration Time (s)	Peak S/N $I$
HD 17081	2453331.5530	12	3800
HD 31293	2453331.6774	140	4050
HD 31648	2453331.6929	319	4225
HD 36112	2453331.7097	320	3725
HD 68695	2453332.7761	640	1950
HD 141569	2453062.8424	1295	5650
HD 142666	2453063.8535	2800	2775
HD 144432	2453062.8983	2100	4575
HD 244604	2453331.6217	1600	4150
HD 245185	2453331.6527	1600	3925
HD 278937	2453330.6795	1860	2550
T Ori	2453332.6371	1440	1900
HD 101412	2453062.7977	1350	1575
HD 190073	2453330.5153	215	3700
V380 Ori	2453330.7576	480	1450

outside the wings on both sides of a Balmer line were carefully chosen, a low order polynomial was then fit through these points, and the polynomial was checked to ensure it varied only a small amount over the Balmer line. In the ESPaDOnS spectra, careful data reduction and the absence of instrumental artifacts produced an excellent correspondence between spectral orders in regions where the orders overlap. These overlap regions were used to evaluate and

minimise errors in normalisation across spectral orders. For stars with both FORS1 and ESPaDOnS spectra available the normalised Balmer lines were compared to ensure the accuracy of the normalisation procedure for ESPaDOnS spectra. A good agreement between the normalised ESPaDOnS and FORS1 Balmer lines was consistently found. In all cases potential normalisation errors are included in the quoted uncertainties of physical parameters.

Careful attention was paid to avoid contamination of the Balmer lines by emission. In our observations the cores of most Balmer lines were partially infilled by emission.  $H\alpha$  was often heavily contaminated by emission, and in many stars was avoided entirely. Despite this, the wings of  $H\gamma$  and  $H\delta$  generally remain free from emission. The wavelength range of possible contamination in the higher Balmer lines can usually be assessed by the more prominent emission in  $H\alpha$ . As a consequence of these complications, the fitting procedure was performed by hand and rather conservative uncertainties were adopted. Synthetic Balmer lines were computed from ATLAS9 (Kurucz 1993) model atmospheres using solar chemical abundances.

Problematically, for many of our stars there is a substantial degeneracy in effective temperature and surface gravity when fitting only the wings of Balmer lines. As a result there is a large covariance between  $T_{\text{eff}}$  and  $\log g$ , and our uncertainties often represent long ellipses in the two dimensional parameter space. Typically these degenerate regions have a slope of +250 K in  $T_{\text{eff}}$  for +0.1 dex in  $\log g$ , though the slope generally becomes steeper towards hotter temperatures.

When good quality fits to the observations were obtainable, fitting of  $T_{\text{eff}}$  and  $\log g$  for the metallic spectra was included in our determination. The fitting procedure is described in Sect. 4. This method relies on the ionisation and excitation balance in the star assuming LTE, but a number of potential problems can occur. Lines with any emission infilling must be avoided. Poor quality atomic data, undiagnosed line blends and non-LTE effects may also be problematic. This also requires lines with a wide range of excitation energies and multiple ionisation states. Consequently, this technique could not successfully be applied to all stars in our sample. In a number of cases the excitation potential could not provide a useful constraint, but the ionisation potential was still useful. In these cases the constraint provided by Balmer line fits, combined with the ionisation balance could still provide fairly precise  $T_{\text{eff}}$  and  $\log g$  values.

In order to place the stars of our sample on the H-R diagram, we needed to determine accurate luminosities. Photometric Johnson  $V$  magnitudes and  $B - V$  colours were derived from the Hipparcos  $V$  magnitudes using the conversion from ESA (1997). For stars without Hipparcos observations, Johnson magnitudes and colours were taken from Vieira et al. (2003), Herbst & Shevchenko (1999), and de Winter et al. (2001). These magnitudes and colours are consistent with those used by Alecian et al. (2012a).

Distance were derived using Hipparcos parallaxes, when available, from the new reduction by van Leeuwen (2007). When no parallax was available, the star was associated with an OB association or star forming region, and a literature distance to that was taken. Associations were taken from Alecian et al. (2012a), which agree with Vieira et al. (2003). Uncertainties for these distances were taken to be the spatial

extent of the associations, which were estimated from their angular size on the sky, assuming the associations are approximately spherical. For HD 169142 no association could reliably be made, and thus a literature photometric distance from Sylvester et al. (1996) was used, and generous uncertainties were assumed. Literature sources for individual distances, along with the distances themselves, can be found in Table, 3.

Using these distances, bolometric luminosities were calculated.  $E(B - V)$  was calculated using the intrinsic colours of Kenyon & Hartmann (1995), and total extinction was calculated using an  $R_V$  of 5, as suggested for HAeBe stars by Hernández et al. (2004). The bolometric correction of Balona (1994) was used.

Using our luminosities and temperatures, we placed the stars on the H-R diagram, as shown in Fig. 1. Pre-main sequence evolutionary tracks and isochrones were calculated with the CESAM (Morel 1997) evolutionary code, assuming solar metallicities. The birth line, the locus of points on the H-R diagram where a star becomes optically visible, was taken from Palla & Stahler (1993), for an accretion rate of  $10^{-5} M_{\odot} \text{yr}^{-1}$ . By comparison to these evolutionary tracks and isochrones, we determined stellar masses, and ages with respect to the birthline. These values, along with fractional pre-main sequence ages ( $\tau$ ) and radii, are presented in Table 3. The uncertainties on mass and age for a star were based on the range of evolutionary tracks and isochrones that intersect the ellipse on the H-R diagram described by the uncertainties in the star's luminosity and  $T_{\text{eff}}$ . Note that the choice of a birthline may introduce a further systematic uncertainty into our ages. For example, using the birthline of Behrend & Maeder (2001), with a mass dependent accretion rate, would generally increase our ages by  $\sim 0.5$  Myr (but with the actual increase varying with mass). While we do not present uncertainties on  $\tau$ , the values should be considered approximate.

## 4 ABUNDANCE ANALYSIS

The abundance analysis and determination of  $v \sin i$  and microturbulence was performed by directly fitting synthetic spectra to the observations. Model spectra were calculated using the ZEEMAN spectrum synthesis code (Landstreet 1988; Wade et al. 2001). This code performs polarised radiative transfer under the assumption of LTE. Optimisations to the code for stars with negligible magnetic fields have been included. A Levenberg-Marquardt  $\chi^2$  minimisation procedure (e.g. Press et al. 1992) was used to determine best fit parameters.

The optimisations to the ZEEMAN spectrum synthesis routine exploit symmetries in a non-magnetic chemically homogeneous model of a star to dramatically reduce the amount of computation required. As in the original version of ZEEMAN, the visible disk of the star is divided into a number of surface elements. In this version it is assumed that the local emergent spectra only vary with projected radial distance from the centre of the disk of the star. Thus radiative transfer is only performed for a set of surface elements with different radial distances, and the results are reused for different angular positions, which minimises the number of times radiative transfer must be performed. The

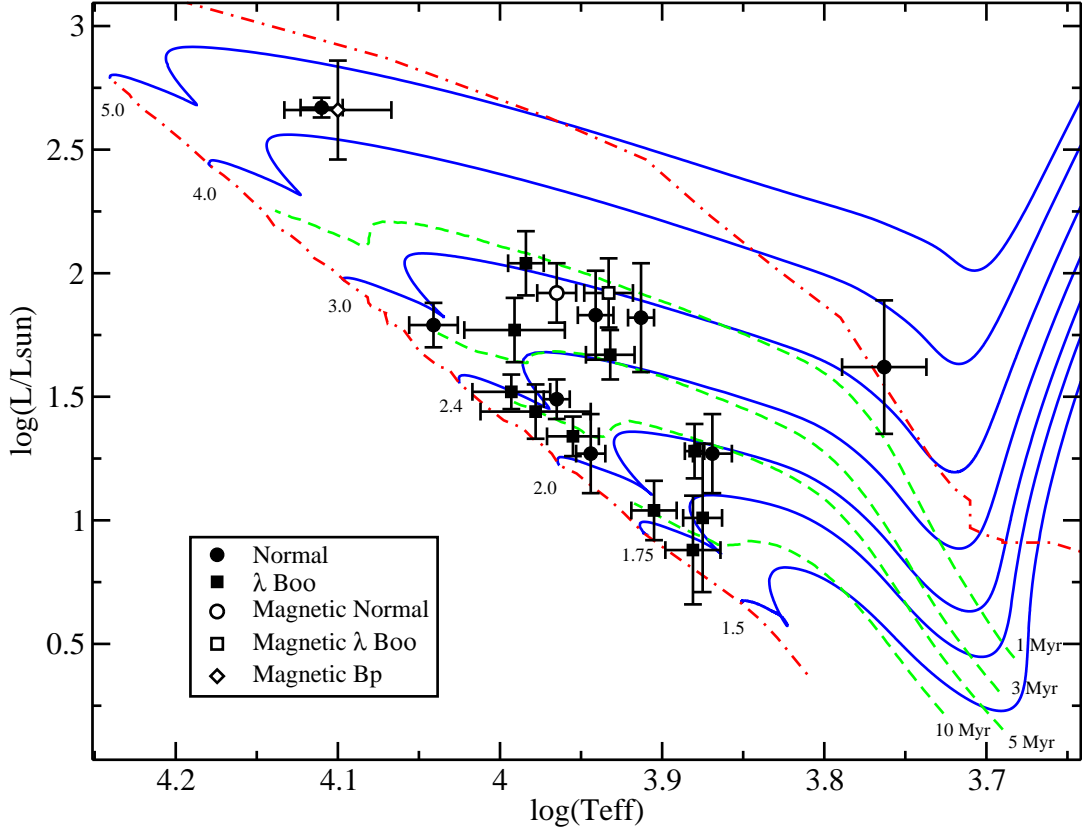


**Figure 1.** H-R diagram for the stars in this study. Evolutionary tracks (solid lines) are labelled by mass in solar masses. Isochrones (dashed lines) are labelled by age in Myr. The birth line (right dot-dashed line) for an accretion rate of  $10^{-5} M_{\odot} \text{ yr}^{-1}$ , and the zero-age main sequence line (ZAMS, left dot-dashed line) are also shown. Circles are chemically normal stars, squares are  $\lambda$  Boo stars, the diamond is the possible Bp star V380 Ori A. Open symbols are stars with confirmed magnetic field detections.

optimisations also assume the local line absorption (Voigt) and anomalous dispersion (Faraday-Voigt) profiles only vary vertically through the atmosphere, and not with position on the stellar disk, substantially reducing the number of times these profiles must be calculated. In this version of the code, limb darkening is still calculated directly, by performing radiative transfer at different radial positions on the disk of the star. Rotational broadening is also calculated directly by summing local emergent spectra that have been Doppler shifted across the disk of the star.

Detailed comparisons of the optimised code to the original version have been performed. For the same input parameters, with no magnetic field, identical spectra are produced. The original code has been checked against other spectrum synthesis codes in detail by Wade et al. (2001), with a very good agreement found. Similarly, the optimised version of ZEEMAN has been checked against SYNTH3 (Kochukhov 2007) and again a good agreement was found.

The Levenberg-Marquardt  $\chi^2$  minimisation procedure (Press et al. 1992) provides a robust and efficient routine for iteratively fitting synthetic spectra to observations. Best fit models from this routine have been compared to fits obtained by hand for a wide variety of stars, and good agreement between the two methods has been consistently found.

Input atomic data were taken from the Vienna Atomic

Line Database (VALD) (Kupka et al. 1999), using an ‘extract stellar’ request and solar chemical abundances. Updated line lists with peculiar abundances were extracted as necessary. Model atmospheres were computed using the ATLAS9 code (Kurucz 1993) with solar abundances. Model atmospheres were calculated on a grid in steps of 250 K in  $T_{\text{eff}}$  and 0.5 in  $\log g$ , then interpolated linearly when more precise values were desired. Interpolation on this grid of models introduces less than 1% relative error to the line depths in the resulting spectrum.

Spectra were initially fit simultaneously for chemical abundances,  $v \sin i$ , microturbulence, and radial velocity, using the best fit  $T_{\text{eff}}$  and  $\log g$  determined from the Balmer lines. Then, if a good constraint could be obtained, the fits were repeated including  $T_{\text{eff}}$  and  $\log g$  as free parameters. If this produced a good fit with well constrained parameters, then these  $T_{\text{eff}}$  and  $\log g$  values were used instead of the initial Balmer line fit values. If only one of  $T_{\text{eff}}$  and  $\log g$  was well constrained from the metallic line fit, then the fit was repeated using the Balmer line value for the unconstrained parameter. We considered a parameter to be well constrained if the fitting routine reliably converged to the same value for different initial conditions, and if that value was consistent with the Balmer line profiles. The fits were generally performed on 5 independent regions  $\sim 500 \text{ \AA}$  long.

**Table 3.** Fundamental parameters derived for the stars in this study.  $\tau$  is the fractional pre-main sequence age. The ‘Magnetic’ column lists which stars have confirmed magnetic field detections (M), and which stars we consider to be non-magnetic (N). The references for distances are: <sup>a</sup>van Leeuwen 2007 (Hipparcos); <sup>b</sup>de Zeeuw et al. 1999; <sup>c</sup>Brown et al. 1994; <sup>d</sup>Dolan & Mathieu 2001; <sup>e</sup>Vieira et al. 2003; <sup>f</sup>Sylvester et al. 1996. The luminosity for HD 190073 was taken from Catala et al. (2007) (indicated by \*).

ID	$T_{\text{eff}}$ (K)	$\log g$	distance (pc)	$\log(L/L_{\odot})$	$M/M_{\odot}$	$R/R_{\odot}$	age (Myr)	$\tau$	Magnetic
HD 17081	$12900 \pm 400$	$3.8 \pm 0.2$	$120 \pm 3^a$	$2.67 \pm 0.04$	$4.4 \pm 0.2$	$4.3 \pm 0.3$	$0.3^{+0.1}_{-0.1}$	0.48	N
HD 31293	$9800 \pm 700$	$3.9 \pm 0.3$	$139 \pm 19^a$	$1.77 \pm 0.13$	$2.55 \pm 0.2$	$2.7 \pm 0.5$	$2.6^{+0.5}_{-0.6}$	0.65	N
HD 31648	$8800 \pm 190$	$4.1 \pm 0.2$	$137 \pm 25^a$	$1.27 \pm 0.16$	$2.1 \pm 0.25$	$1.9 \pm 0.4$	$6.2^{+4.0}_{-2.0}$	0.84	N
HD 36112	$8190 \pm 150$	$4.1 \pm 0.4$	$279 \pm 70^a$	$1.82 \pm 0.22$	$2.8 \pm 0.5$	$4.0 \pm 1.0$	$1.5^{+1.5}_{-1.0}$	0.52	N
HD 68695	$9000 \pm 300$	$4.3 \pm 0.3$	$410 \pm 36^b$	$1.34 \pm 0.08$	$2.2 \pm 0.15$	$1.9 \pm 0.2$	$5.2^{+3.0}_{-1.0}$	0.76	N
HD 139614	$7600 \pm 300$	$3.9 \pm 0.3$	$147 \pm 37^b$	$0.88 \pm 0.22$	$1.7 \pm 0.1$	$1.6 \pm 0.4$	$13.5^{+11}_{-5.0}$	0.82	N
HD 141569	$9800 \pm 500$	$4.2 \pm 0.4$	$116 \pm 8^a$	$1.52 \pm 0.07$	$2.4 \pm 0.2$	$2.0 \pm 0.3$	$4.0^{+1.5}_{-1.0}$	0.83	N
HD 142666	$7500 \pm 200$	$3.9 \pm 0.3$	$145 \pm 18^b$	$1.28 \pm 0.11$	$1.95 \pm 0.15$	$2.5 \pm 0.3$	$6.0^{+1.0}_{-1.5}$	0.63	N
HD 144432	$7400 \pm 200$	$3.9 \pm 0.3$	$160 \pm 29^a$	$1.27 \pm 0.16$	$1.95 \pm 0.2$	$2.6 \pm 0.5$	$5.5^{+2.5}_{-1.5}$	0.58	N
HD 163296	$9200 \pm 300$	$4.2 \pm 0.3$	$119 \pm 11^a$	$1.49 \pm 0.08$	$2.3 \pm 0.1$	$2.2 \pm 0.2$	$4.1^{+1.0}_{-0.2}$	0.71	N
HD 169142	$7500 \pm 200$	$4.3 \pm 0.2$	$145 \pm 50^f$	$1.01 \pm 0.30$	$1.7 \pm 0.2$	$1.9 \pm 0.7$	$8.5^{+16}_{-3.0}$	0.52	N
HD 176386	$11000 \pm 400$	$4.1 \pm 0.3$	$128 \pm 13^a$	$1.79 \pm 0.09$	$2.8 \pm 0.2$	$2.2 \pm 0.3$	$2.7^{+1.0}_{-1.0}$	0.93	N
HD 179218	$9640 \pm 250$	$3.9 \pm 0.2$	$254 \pm 38^a$	$2.04 \pm 0.13$	$3.1 \pm 0.3$	$3.7 \pm 0.6$	$1.1^{+0.7}_{-0.6}$	0.55	N
HD 244604	$8700 \pm 220$	$4.0 \pm 0.2$	$380 \pm 79^c$	$1.83 \pm 0.18$	$2.75 \pm 0.4$	$3.6 \pm 0.8$	$1.9^{+1.1}_{-1.0}$	0.61	N
HD 245185	$9500 \pm 750$	$4.0 \pm 0.4$	$450 \pm 50^d$	$1.44 \pm 0.11$	$2.3 \pm 0.2$	$1.9 \pm 0.4$	$5.5^{+2.0}_{-2.0}$	0.90	N
HD 278937	$8000 \pm 250$	$4.1 \pm 0.2$	$318 \pm 43^b$	$1.04 \pm 0.12$	$1.8 \pm 0.1$	$1.7 \pm 0.3$	$9.5^{+5.0}_{-3.0}$	0.76	N
T Ori	$8500 \pm 300$	$4.2 \pm 0.3$	$380 \pm 44^c$	$1.67 \pm 0.10$	$2.45 \pm 0.15$	$3.1 \pm 0.4$	$3.3^{+1.2}_{-1.3}$	0.75	N
HD 101412	$8600 \pm 300$	$4.0 \pm 0.5$	$600 \pm 100^e$	$1.92 \pm 0.14$	$3.0 \pm 0.3$	$4.2 \pm 0.8$	$1.2^{+0.8}_{-0.6}$	0.50	M
HD 190073	$9230 \pm 260$	$3.7 \pm 0.3$	$> 340^a$	$1.92 \pm 0.12^*$	$2.9 \pm 0.3$	$3.6 \pm 0.5$	$1.6^{+0.7}_{-0.6}$	0.62	M
V380 Ori A	$12600 \pm 1000$	$4.0 \pm 0.5$	$398 \pm 91^c$	$2.66 \pm 0.20$	$4.4 \pm 0.7$	$4.5 \pm 1.2$	$0.4^{+0.6}_{-0.3}$	0.55	M
V380 Ori B	$5800 \pm 350$	$4.1 \pm 0.3$	$398 \pm 91^c$	$1.62 \pm 0.27$	$3.3 \pm 0.8$	$6.4 \pm 2.2$	$0.0^{+1.5}_{-1.5}$	0.0	N

The approximate wavelength ranges usually were 4400-4800, 4900-5500, 5500-6000, 6000-6500, and 6600-7600 Å, and occasionally 4150-4280 Å, with significant gaps due to non-photospheric features. These windows typically contained several hundred spectral lines (the number varying greatly with wavelength and  $T_{\text{eff}}$ ), however many of these lines are very weak and hence do not provide significant constraints on the best fit abundances or atmospheric parameters. The exact wavelength ranges varied between stars, due to varying regions of emission and different Balmer line widths.

Microturbulence and  $v \sin i$  were determined by  $\chi^2$  minimisation, simultaneously with the other stellar parameters, using the entire spectral  $\sim 500$  Å window. This method relies on resolved, rotationally broadened spectral lines for constraining  $v \sin i$ , and a range of both weak and strong lines for constraining microturbulence.

We verified this method of determining  $T_{\text{eff}}$  and  $\log g$  by analysing well studied stars, and comparing to literature results. In this study we have analysed  $\pi$  Cet, and compared our results with the very precise study by Fossati et al. (2009). Fossati et al. (2009) used photometry and spectral energy distributions, as well as Balmer lines, and excitation and ionisation balances when determining their parameters. They also used different software tools to perform their modelling, thus their results are truly independent. Our results are fully consistent with theirs, as discussed in Sect. A1, which demonstrates the accuracy of our methodology.

For this method to be successful, lines contaminated by emission must be avoided. While a line entirely in emission is easily identified, lines with small amounts of emission infilling are harder to identify. When multiple observations were

available, variability in the emission could be used to identify lines with emission infilling. If only one observation was available, special attention was paid to lines with low excitation potentials and large oscillator strengths, such lines being more likely to contain emission. If inconsistent fits were obtained between normal and low excitation potential lines, and no other clear explanation for the inconsistency could be found (such as an error in  $T_{\text{eff}}$  or the atomic data), the low excitation potential lines were considered to likely contain emission and were excluded from the final fit. Additionally, the shapes of line profiles were examined and, if they could not be reproduced by the synthetic spectra, they were considered to be contaminated by a non-photospheric component. The presence of veiling in our spectra is assessed in detail in Section 6.4, and we find it is not present at a significant level.

The use of multiple spectral windows is valuable, as it allows us to take the average and standard deviation of abundances determined across the windows. The standard deviation in particular provides a reasonable estimate of the uncertainty of derived parameters. Since line-to-line abundances scatter is introduced by errors in the atomic data as well as errors in the model atmosphere, these effects are included in the standard deviation. The standard deviation may underestimate the impact of such errors, but provides a robust and easily understandable uncertainty estimate. The use of multiple spectral windows also allows us to verify the atmospheric parameters derived from metal line fits. If the parameters differ substantially from window to window, they are likely poorly constrained in some if not all windows,

in which case we can rely more heavily on the parameters from Balmer line fitting.

For chemical elements with fewer than four lines providing good constraints on the abundance in any spectral window (including all cases of elements with lines in only one or two spectral windows) the uncertainties were estimated by eye rather than using a standard deviation. These uncertainties were chosen to include line-to-line scatter, uncertainties in the atmospheric parameters, and potential normalisation errors.

Examples of typical best fit synthetic spectra compared to the observed spectrum of HD 139614 in the 5000-5050 Å and 6100-6200 Å windows are presented in Fig. 2. Final averaged best fit abundances and atmospheric parameters are presented in Table 4, together with uncertainties. Elements with abundances based on less than four lines are indicated with an asterisk in the table.

We find 11 stars with varying degrees of  $\lambda$  Boo peculiarity, one star (V380 Ori A) that appears to be a weak Ap/Bp star, and 9 stars that are chemically normal (although results for V380 Ori B are very uncertain). The properties of the individual stars are discussed in detail in the Appendix. The final best fit abundances are plotted relative to solar abundances from Grevesse et al. (2005) in Figures A2, A3, A4, and A5. Illustrations of our fits for all of the stars in our study can be found in Figures A6 to A25.

## 5 TRENDS

In order to investigate trends in chemical abundance relative to other stellar parameters, we constructed a peculiarity index to describe whether a star is chemically normal, more like a  $\lambda$  Boo star, or more like an Ap/Bp star. This index is designed to be positive for stars with overabundances of iron peak elements, zero for chemically normal stars, and negative for stars underabundant in iron peak elements. The peculiarity index is the difference between the average of the Cr, Fe, and Ni abundances relative to solar and the average of the C, N, and O abundances relative to solar. Specifically, the index is calculated as:

$$[P] = \frac{1}{3} \left( ([\text{Cr}] + [\text{Fe}] + [\text{Ni}]) - ([\text{C}] + [\text{N}] + [\text{O}]) \right), \quad (1)$$

where the abundances are relative to solar:  $[X] = \log(N_{X,*}/N_{tot,*}) - \log(N_{X,\odot}/N_{tot,\odot})$ . These particular elements were chosen because they tend to have peculiar abundances in chemically peculiar stars (for Cr, Fe, and Ni) or normal abundances in chemically normal stars (for C, N and O). These elements were also chosen because reliable abundances for them are available for most stars in our sample. In the few cases in which we could not determine an abundance for an element used in the peculiarity index, that element was left out of the average.

We plotted the index  $[P]$  against effective temperature, mass, age, and fractional pre-main sequence age, as shown in Fig. 3. No clear trends were found, with a large scatter in chemical abundance at most temperatures, masses, and ages. This peculiarity index was also compared to stellar radius,  $v \sin i$ , and microturbulence, but again no clear trends were found. Thus we conclude that the  $\lambda$  Boo peculiarities that we see are not restricted to a narrow mass range, and that they are present throughout the pre-main sequence.

## 6 DISCUSSION

### 6.1 $\lambda$ Boo peculiarities

The most striking result of this study is the discovery of a large number of HAeBe stars with moderate  $\lambda$  Boo type chemical peculiarities. This trend seems to be present in both stars with and without detected magnetic fields, as shown by HD 101412. We find 7 stars showing fairly strong  $\lambda$  Boo peculiarities, and another 4 stars with weaker  $\lambda$  Boo peculiarities, while 8 stars are chemically normal and 1 is rather uncertain but appears to be normal. With the derived abundances, we see a continuous distribution of  $\lambda$  Boo peculiarities, from fairly strong to nearly undetectable. This incidence of roughly 50% is much higher than the incidence of  $\lambda$  Boo stars on the main sequence of roughly 2% (Paunzen 2001). While a detection rate of 50% may be an overestimate (since our sample is biased towards stars with limited emission in their optical spectra), the true incidence of  $\lambda$  Boo peculiarities in HAeBe stars certainly is much higher than observed on the main sequence, suggesting an important connection with the pre-main sequence evolutionary phase.

The sample of stars in our study is biased towards stars with weaker circumstellar emission or absorption in their spectra, since these stars allow for a more complete analysis of their photospheric spectra. However, the stars were drawn from the larger sample of Alecian et al. (2012a) which did not have this bias. We found 65% of the stars in their sample had modest amounts of circumstellar contamination, and would have been suitable for our photospheric analysis. Thus, as a lower limit, 33% of HAeBe stars should show  $\lambda$  Boo peculiarities, assuming that all the unsuitable stars in the sample of Alecian et al. (2012a) are chemically normal, and using our derived incidence of peculiarities for the suitable stars. The true incidence is likely higher than this lower limit.

There are almost certainly more undetected  $\lambda$  Boo stars in the sample of Alecian et al. (2012a) that we did not analyse, simply because analysing their complete sample was beyond the scope of this study. Indeed Alecian et al. (2012a) mention that HD 34282 appears to have weak lines of iron peak elements, but a normal O line. To roughly estimate the number of potential  $\lambda$  Boo stars in the remaining sample, we compared synthetic spectra computed using literature values for their atmospheric parameters and assuming solar abundances with the ESPaDOnS observations. In doing so we identified 5 additional stars that have suspiciously weak metal lines for their literature temperatures: HD 37806, HD 98922, HD 144668, HD 76534, and VX Cas. If all these stars do indeed show  $\lambda$  Boo peculiarities, 35% of the stars observed with ESPaDOnS by Alecian et al. (2012a) would be  $\lambda$  Boo stars, which is consistent with our results.

This large incidence of  $\lambda$  Boo type peculiarities in HAeBe stars is qualitatively consistent with a selective accretion model of  $\lambda$  Boo stars. HAeBe stars have recently undergone accretion, and may still be accreting, so it is reasonable that a process which depends on accretion is seen more frequently in these stars. Thus we consider our results supportive of the selective accretion model of  $\lambda$  Boo stars.

The large number of pre-main sequence  $\lambda$  Boo stars we find suggests that the majority of  $\lambda$  Boo stars may develop their peculiarities on the pre-main sequence by accreting their circumstellar material. However, we cannot rule out

**Table 4.** Best fit parameters for the stars in our sample. Chemical abundances are in units of  $\log(N_X/N_{tot})$ . Elements marked with an asterisk are based on less than  $\sim 4$  useful lines and have uncertainties estimated by eye. Microturbulence is given by  $\xi$ .

	HD 17081 ( $\pi$ Cet)	HD 31293 (AB Aur)	HD 31648	HD 36112	HD 68695	HD 139614	HD 141569	Solar
$T_{\text{eff}}$ (K)	$12900 \pm 400$	$9800 \pm 700$	$8800 \pm 190$	$8190 \pm 150$	$9000 \pm 300$	$7600 \pm 300$	$9800 \pm 500$	
$\log g$ (cgs)	$3.8 \pm 0.2$	$3.9 \pm 0.3$	$4.1 \pm 0.2$	$4.1 \pm 0.4$	$4.3 \pm 0.3$	$3.9 \pm 0.3$	$4.2 \pm 0.4$	
$v \sin i$ ( $\text{km s}^{-1}$ )	$20.9 \pm 1.2$	$116 \pm 9$	$101.2 \pm 1.7$	$57.8 \pm 1.0$	$51 \pm 4$	$25.6 \pm 0.4$	$222 \pm 7$	
$\xi$ ( $\text{km s}^{-1}$ )	$1.7 \pm 1.0$	$\leq 4$	$3.2 \pm 1.1$	$2.97 \pm 0.24$	$1.3 \pm 1.1$	$3.7 \pm 0.4$	$\leq 2$	
He	$-0.91 \pm 0.14$	$-1.24 \pm 0.20^*$					$-1.21 \pm 0.37^*$	$-1.11$
C	$\leq -3.4^*$	$-3.33 \pm 0.22$	$-3.67 \pm 0.07$	$-3.61 \pm 0.16$	$-3.27 \pm 0.18$	$-3.75 \pm 0.22$	$-3.63 \pm 0.29$	$-3.65$
N	$-4.03 \pm 0.15^*$	$-3.9 \pm 0.3^*$			$-3.7 \pm 0.3^*$	$-4.17 \pm 0.13$	$-4.0 \pm 0.3^*$	$-4.26$
O	$-3.16 \pm 0.13$	$-3.27 \pm 0.20$	$-3.28 \pm 0.05^*$	$-3.18 \pm 0.10^*$	$-3.17 \pm 0.10$	$-3.33 \pm 0.10^*$	$-3.05 \pm 0.10$	$-3.38$
Ne	$-3.76 \pm 0.28$							$-4.20$
Na	$-5.30 \pm 0.10^*$		$-5.72 \pm 0.25^*$	$-5.58 \pm 0.15^*$	$-6.2 \pm 0.4^*$	$-6.14 \pm 0.12$	$\leq -5.2^*$	$-5.87$
Mg	$-4.43 \pm 0.15$	$-4.89 \pm 0.33$	$-4.12 \pm 0.13$	$-4.23 \pm 0.14$	$-5.11 \pm 0.14$	$-4.74 \pm 0.07$	$-4.90 \pm 0.11$	$-4.51$
Al	$-5.81 \pm 0.17$						$-5.6 \pm 0.5^*$	$-5.67$
Si	$-4.55 \pm 0.14$	$-4.76 \pm 0.22$	$-4.29 \pm 0.19$	$-4.58 \pm 0.11$	$-5.36 \pm 0.15$	$-5.10 \pm 0.13$	$-4.99 \pm 0.31$	$-4.53$
P	$-6.43 \pm 0.14$							$-6.68$
S	$-4.99 \pm 0.08$		$-4.6 \pm 0.3^*$	$-4.79 \pm 0.16^*$	$-4.6 \pm 0.3^*$	$-5.18 \pm 0.15$		$-4.90$
Ar	$-5.6 \pm 0.3^*$							$-5.86$
K						$-7.29 \pm 0.25^*$		$-6.96$
Ca	$-5.7 \pm 0.2^*$	$-6.10 \pm 0.17$	$-5.38 \pm 0.23$	$-5.59 \pm 0.16$	$-6.47 \pm 0.23$	$-6.18 \pm 0.16$	$-6.34 \pm 0.38$	$-5.73$
Sc		$-9.04 \pm 0.34$	$-8.72 \pm 0.15$	$-8.90 \pm 0.26$	$-9.49 \pm 0.26$	$-9.39 \pm 0.15$	$-9.18 \pm 0.37$	$-8.87$
Ti	$-7.37 \pm 0.15$	$-7.47 \pm 0.27$	$-6.82 \pm 0.09$	$-6.98 \pm 0.20$	$-7.71 \pm 0.25$	$-7.51 \pm 0.14$	$-7.74 \pm 0.32$	$-7.14$
V				$-7.8 \pm 0.4^*$		$-8.4 \pm 0.5^*$		$-8.04$
Cr	$-6.57 \pm 0.16$	$-6.67 \pm 0.27$	$-6.09 \pm 0.17$	$-6.30 \pm 0.17$	$-6.98 \pm 0.24$	$-6.80 \pm 0.11$	$-7.31 \pm 0.31$	$-6.40$
Mn	$-6.6 \pm 0.3^*$		$-6.59 \pm 0.08$	$-6.70 \pm 0.16$	$-6.4 \pm 0.5^*$	$-7.43 \pm 0.19$		$-6.65$
Fe	$-4.70 \pm 0.08$	$-4.91 \pm 0.25$	$-4.47 \pm 0.13$	$-4.49 \pm 0.14$	$-5.16 \pm 0.22$	$-5.07 \pm 0.13$	$-5.25 \pm 0.32$	$-4.59$
Co								$-7.12$
Ni	$-5.85 \pm 0.06$	$-6.16 \pm 0.27$	$-5.66 \pm 0.05$	$-5.76 \pm 0.20$	$-6.25 \pm 0.32$	$-6.33 \pm 0.14$	$\leq -6.0^*$	$-5.81$
Cu				$\leq -7.5^*$		$-8.6 \pm 0.4^*$		$-7.83$
Zn				$-7.8 \pm 0.4^*$		$-8.3 \pm 0.3^*$		$-7.44$
Sr		$-9.6 \pm 0.3^*$		$-9.4 \pm 0.3^*$			$-10.5 \pm 0.5^*$	$-9.12$
Y			$-9.57 \pm 0.30$	$-9.56 \pm 0.17$		$-10.23 \pm 0.15$		$-9.83$
Zr				$-9.3 \pm 0.3^*$				$-9.48$
Ba		$-9.7 \pm 0.4^*$	$-9.56 \pm 0.24^*$	$-9.46 \pm 0.29$	$-10.3 \pm 0.4^*$	$-10.29 \pm 0.21$	$-9.2 \pm 0.8^*$	$-9.87$
La								$-10.91$
Ce						$\leq -10.5^*$		$-10.34$
Nd								$-10.59$
Eu								$-11.52$
	HD 142666	HD 144432	HD 163296	HD 169142	HD 176386	HD 179218	HD 244604	Solar
$T_{\text{eff}}$ (K)	$7500 \pm 200$	$7400 \pm 200$	$9200 \pm 300$	$7500 \pm 200$	$11000 \pm 400$	$9640 \pm 250$	$8700 \pm 220$	
$\log g$ (cgs)	$3.9 \pm 0.3$	$3.9 \pm 0.3$	$4.2 \pm 0.3$	$4.3 \pm 0.2$	$4.1 \pm 0.3$	$3.9 \pm 0.2$	$4.0 \pm 0.2$	
$v \sin i$ ( $\text{km s}^{-1}$ )	$68.0 \pm 0.9$	$80.3 \pm 1.0$	$122 \pm 3$	$51.6 \pm 0.5$	$169.0 \pm 1.5$	$70 \pm 4$	$101 \pm 5$	
$\xi$ ( $\text{km s}^{-1}$ )	$3.55 \pm 0.31$	$3.62 \pm 0.23$	$1.5 \pm 1.2$	$2.09 \pm 0.47$	$1.7 \pm 0.7$	$2.0 \pm 0.5$	$1.9 \pm 0.4$	
He					$-1.17 \pm 0.20^*$	$-1.15 \pm 0.15^*$		$-1.11$
C	$-3.62 \pm 0.15$	$-3.79 \pm 0.18$	$-3.82 \pm 0.25$	$-3.55 \pm 0.12$	$-3.38 \pm 0.29^*$	$-3.45 \pm 0.16$	$-3.69 \pm 0.17$	$-3.65$
N					$-3.9 \pm 0.3^*$	$-3.5 \pm 0.4^*$	$-4.2 \pm 0.3^*$	$-4.26$
O	$-3.18 \pm 0.15^*$	$-3.17 \pm 0.10^*$	$-3.31 \pm 0.15$	$-3.38 \pm 0.13$	$-3.20 \pm 0.10^*$	$-3.10 \pm 0.13$	$-3.23 \pm 0.08$	$-3.38$
Ne								$-4.20$
Na	$-5.77 \pm 0.15^*$	$-5.86 \pm 0.09$	$-5.6 \pm 0.5^*$	$-6.18 \pm 0.08^*$		$-5.5 \pm 0.3^*$	$-5.4 \pm 0.3^*$	$-5.87$
Mg	$-4.61 \pm 0.06$	$-4.46 \pm 0.04$	$-4.12 \pm 0.15$	$-4.89 \pm 0.06$	$-4.28 \pm 0.15$	$-4.73 \pm 0.17$	$-4.03 \pm 0.22$	$-4.51$
Al			$-5.5 \pm 0.4^*$		$-5.5 \pm 0.3^*$	$-6.0 \pm 0.4^*$		$-5.67$
Si	$-4.91 \pm 0.20$	$-4.81 \pm 0.24$	$-4.24 \pm 0.14$	$-5.13 \pm 0.10$	$-4.44 \pm 0.14$	$-4.82 \pm 0.22$	$-4.34 \pm 0.06$	$-4.53$
P								$-6.68$
S	$-4.70 \pm 0.15$	$-4.82 \pm 0.05$		$-5.10 \pm 0.12$		$-4.2 \pm 0.4^*$	$-4.48 \pm 0.15^*$	$-4.90$
Ar								$-5.86$
K								$-6.96$
Ca	$-5.98 \pm 0.18$	$-5.78 \pm 0.15$	$-5.54 \pm 0.30$	$-6.15 \pm 0.12$	$-6.27 \pm 0.19^*$	$-6.25 \pm 0.38$	$-5.42 \pm 0.24$	$-5.73$
Sc	$-9.23 \pm 0.23$	$-9.09 \pm 0.15$	$-8.76 \pm 0.08$	$-9.58 \pm 0.24$	$-9.0 \pm 0.4^*$	$-9.40 \pm 0.16$	$-8.75 \pm 0.24$	$-8.87$
Ti	$-7.39 \pm 0.20$	$-7.26 \pm 0.16$	$-6.92 \pm 0.10$	$-7.65 \pm 0.10$	$-7.12 \pm 0.29$	$-7.57 \pm 0.12$	$-6.81 \pm 0.31$	$-7.14$
V	$-8.4 \pm 0.4^*$	$-8.3 \pm 0.4^*$		$-8.49 \pm 0.16^*$				$-8.04$
Cr	$-6.60 \pm 0.21$	$-6.51 \pm 0.23$	$-5.95 \pm 0.20$	$-6.98 \pm 0.13$	$-6.46 \pm 0.21$	$-6.97 \pm 0.13$	$-6.07 \pm 0.16$	$-6.40$
Mn	$-7.08 \pm 0.15$	$-6.96 \pm 0.15$	$-7.0 \pm 0.5^*$	$-7.57 \pm 0.20$			$-6.91 \pm 0.23$	$-6.65$
Fe	$-4.84 \pm 0.11$	$-4.70 \pm 0.09$	$-4.39 \pm 0.15$	$-5.13 \pm 0.11$	$-4.48 \pm 0.27$	$-5.03 \pm 0.13$	$-4.35 \pm 0.24$	$-4.59$
Co	$-6.8 \pm 0.4^*$	$-7.1 \pm 0.5^*$		$\leq -7.6^*$				$-7.12$
Ni	$-6.16 \pm 0.13$	$-6.00 \pm 0.15$	$-5.72 \pm 0.12$	$-6.40 \pm 0.16$		$\leq -5.9^*$	$-6.00 \pm 0.18$	$-5.81$
Cu		$\leq -7.7^*$		$-8.85 \pm 0.28$				$-7.83$
Zn	$-7.9 \pm 0.3^*$	$-7.57 \pm 0.20$		$-8.71 \pm 0.08^*$				$-7.44$
Sr	$-9.56 \pm 0.19^*$	$-9.4 \pm 0.3^*$		$-9.58 \pm 0.11^*$		$-10.2 \pm 0.2^*$		$-9.12$
Y	$-9.94 \pm 0.22$	$-9.80 \pm 0.13$		$-10.18 \pm 0.14$		$-10.0 \pm 0.4^*$	$-9.8 \pm 0.4^*$	$-9.83$
Zr	$-9.36 \pm 0.26^*$	$-9.3 \pm 0.4^*$		$-9.65 \pm 0.13^*$				$-9.48$
Ba	$-9.81 \pm 0.18$	$-9.69 \pm 0.16$	$-10.0 \pm 0.4^*$	$-9.96 \pm 0.21$	$\leq -9.0^*$	$-10.4 \pm 0.4^*$	$-9.6 \pm 0.2^*$	$-9.87$
La	$\leq -10.8^*$	$-11.2 \pm 0.4^*$						$-10.91$
Ce								$-10.34$
Nd				$-10.64 \pm 0.14^*$				$-10.59$
Eu				$-12.19 \pm 0.10^*$				$-11.52$

**Table 4** – *continued* Best fit parameters for the stars in our sample. Chemical abundances are in units of  $\log(N_X/N_{tot})$ . Elements marked with an asterisk are based on less than  $\sim 4$  useful lines and have uncertainties estimated by eye. Microturbulence is given by  $\xi$ .

	HD 245185	HD 278937 (IP Per)	T Ori (BD -05 1329)	HD 101412	HD 190073	V380 Ori A	V380 Ori B	Solar
$T_{\text{eff}}$ (K)	$9500 \pm 750$	$8000 \pm 250$	$8500 \pm 300$	$8600 \pm 300$	$9230 \pm 260$	$12600 \pm 1000$	$5800 \pm 350$	
$\log g$ (cgs)	$4.0 \pm 0.4$	$4.1 \pm 0.2$	$4.2 \pm 0.3$	$4.0 \pm 0.5$	$3.7 \pm 0.3$	$4.0 \pm 0.5$	$4.1 \pm 0.3$	
$v \sin i$ ( $\text{km s}^{-1}$ )	$136 \pm 10$	$83.8 \pm 4.6$	$163 \pm 11$	$6.8 \pm 0.4$	$8.50 \pm 0.23$	$9.9 \pm 1.0$	$24.7 \pm 1.9$	
$\xi$ ( $\text{km s}^{-1}$ )	$\leq 4$	$2.0 \pm 0.9$	$2.6 \pm 1.1$	$\leq 2$	$\leq 2$	$\leq 3$	$\leq 2$	
He	$-0.9 \pm 0.3^*$		$-1.4 \pm 0.5^*$	$-0.9 \pm 0.3^*$	$-0.90 \pm 0.20^*$	$-0.67 \pm 0.20^*$		-1.11
C	$-3.72 \pm 0.15$	$-3.57 \pm 0.17$	$-3.59 \pm 0.19$	$-3.58 \pm 0.12$	$-3.72 \pm 0.14$	$-3.4 \pm 0.4^*$		-3.65
N	$-3.8 \pm 0.4^*$	$-4.0 \pm 0.3^*$	$-4.2 \pm 0.4^*$		$-3.60 \pm 0.20^*$			-4.26
O	$-3.17 \pm 0.17$	$-3.41 \pm 0.05$	$-3.16 \pm 0.12$	$-3.12 \pm 0.09$	$-3.26 \pm 0.11$	$-3.00 \pm 0.16$		-3.38
Ne					$-3.8 \pm 0.3^*$	$-3.93 \pm 0.36$		-4.20
Na		$-6.3 \pm 0.3^*$	$-6.1 \pm 0.3^*$	$-5.56 \pm 0.15^*$	$-5.13 \pm 0.15^*$		$-5.95 \pm 0.30^*$	-5.87
Mg	$-5.39 \pm 0.23$	$-4.91 \pm 0.11$	$-5.05 \pm 0.23$	$-4.95 \pm 0.15$	$-4.38 \pm 0.17$	$-4.19 \pm 0.14$	$-4.7 \pm 0.7^*$	-4.51
Al	$-5.4 \pm 0.5^*$		$-5.2 \pm 0.4^*$	$-5.99 \pm 0.20^*$	$-5.58 \pm 0.17^*$	$-5.07 \pm 0.21^*$		-5.67
Si	$-4.95 \pm 0.16$	$-4.97 \pm 0.19$	$-4.89 \pm 0.20$	$-5.30 \pm 0.19$	$-4.48 \pm 0.06$	$-4.11 \pm 0.09$	$-4.44 \pm 0.26$	-4.53
P						$-5.86 \pm 0.30^*$		-6.68
S		$-4.83 \pm 0.14$	$-4.1 \pm 0.3^*$	$-4.96 \pm 0.12$	$-4.57 \pm 0.20^*$	$-4.93 \pm 0.26$		-4.90
Ar								-5.86
K								-6.96
Ca	$-6.12 \pm 0.25$	$-6.28 \pm 0.18$	$-6.00 \pm 0.31$	$-6.37 \pm 0.20$	$-5.61 \pm 0.12$	$\leq -5.6^*$	$-5.78 \pm 0.40$	-5.73
Sc	$-9.6 \pm 0.7^*$	$-9.52 \pm 0.21$	$-9.4 \pm 0.3^*$	$-9.33 \pm 0.17$	$-8.85 \pm 0.20$			-8.87
Ti	$-7.93 \pm 0.38$	$-7.81 \pm 0.10$	$-7.55 \pm 0.17$	$-7.75 \pm 0.23$	$-7.16 \pm 0.12$		$-6.78 \pm 0.28$	-7.14
V	$\leq -7.5^*$			$-8.1 \pm 0.3^*$	$-7.99 \pm 0.25^*$		$-7.50 \pm 0.79$	-8.04
Cr	$-7.27 \pm 0.34$	$-7.04 \pm 0.18$	$-6.82 \pm 0.07$	$-6.69 \pm 0.29$	$-6.13 \pm 0.13$	$\leq -4.8^*$	$-5.92 \pm 0.26$	-6.40
Mn	$-7.0 \pm 0.6^*$	$-7.3 \pm 0.4^*$	$\leq -6.0^*$	$-6.98 \pm 0.09$	$-6.54 \pm 0.08$	$-5.92 \pm 0.16$	$-5.97 \pm 0.43$	-6.65
Fe	$-5.27 \pm 0.33$	$-5.12 \pm 0.16$	$-4.98 \pm 0.10$	$-5.08 \pm 0.19$	$-4.42 \pm 0.06$	$-3.92 \pm 0.12$	$-4.25 \pm 0.16$	-4.59
Co							$-6.6 \pm 0.6^*$	-7.12
Ni	$-6.5 \pm 0.7^*$	$-6.37 \pm 0.22$		$-6.13 \pm 0.27$	$-5.69 \pm 0.17$	$-5.19 \pm 0.18$	$-5.58 \pm 0.32$	-5.81
Cu		$\leq -7.5^*$		$-8.6 \pm 0.3^*$			$-7.4 \pm 0.7^*$	-7.83
Zn		$\leq -8.0^*$			$-7.52 \pm 0.25^*$		$-7.4 \pm 0.6^*$	-7.44
Sr			$-9.3 \pm 0.2^*$					-9.12
Y		$-10.4 \pm 0.4^*$		$-10.12 \pm 0.25$	$-9.70 \pm 0.20$		$\leq -8.2^*$	-9.83
Zr				$-9.8 \pm 0.3^*$	$-9.2 \pm 0.3^*$			-9.48
Ba	$-10.0 \pm 0.7^*$	$-10.2 \pm 0.3^*$	$-10.3 \pm 0.3^*$	$-10.71 \pm 0.24$	$-9.71 \pm 0.13^*$		$-8.89 \pm 0.40$	-9.87
La								-10.91
Ce					$\leq -9.6^*$		$\leq -8.5^*$	-10.34
Nd					$-10.2 \pm 0.3^*$			-10.59
Eu								-11.52

the existence more of evolved  $\lambda$  Boo stars that only develop peculiarities on the main sequence, by accreting from diffuse interstellar clouds. Due to the relatively short lifetime of  $\lambda$  Boo peculiarities after accretion has halted, the presence of such peculiarities later in the main sequence (e.g. Paunzen et al. 2002) may require a different source of accreted material from that of pre-main sequence  $\lambda$  Boo stars.

Turcotte & Charbonneau (1993) modelled the diffusion of chemical elements in the atmosphere of a star (with  $T_{\text{eff}} = 8000$  K and  $\log g = 4.3$ ) that was accreting gas depleted in iron peak elements. They found that  $\lambda$  Boo peculiarities can be generated quickly ( $\sim 0.1$  Myr), but also dissipate quickly after accretion has stopped ( $\sim 1$  Myr). This implies that, in the context of selective accretion, there is a good chance that HAeBe stars with  $\lambda$  Boo peculiarities are still accreting, or were very recently accreting.

The range in strengths of the  $\lambda$  Boo peculiarities seen in the stars in our sample might be interpreted as the consequence of different accretion rates in the stars. However, Turcotte & Charbonneau (1993) do not find a strong impact on surface abundances from different accretion rates, as long as they are sufficient to overwhelm diffusion and rotational mixing.

Alternately, the differences in the strengths of peculiarities could reflect the abundances of the accreted gas. These differences being due, for example, to the efficiency with which iron peak elements are bound into dust grains, or to

the degree to which dust is blown away from the star while gas is accreted.

In this context, the chemically normal stars are most likely not accreting significant amounts of material, and thus any  $\lambda$  Boo peculiarities have dissipated. However, it is possible that accretion is ongoing but the selection process in the circumstellar material has broken down. For example, dust grain formation may not be proceeding efficiently, and thus the accreted gas would not be depleted in iron peak elements

Unfortunately, deriving accretion rates for HAeBe stars is not a simple process. For example, Donehew & Brittain (2011) measured accretion rates based on Balmer jump excess fluxes. They obtained values between a few  $10^{-7}$  and  $10^{-8} M_{\odot} \text{yr}^{-1}$ . These values rely on models from Muzerolle et al. (2004), which are constructed assuming magnetospheric accretion. Given the absence of detectable magnetic fields in most of the stars in our study, magnetospheric accretion may not be an accurate model (see Wade et al. 2007), and thus these accretion rates may not be accurate either. Generally, accretion rates derived for HAeBe stars are based on rather simple models, and thus it is not clear how reliable those accretion rates are. Eleven of the stars in our sample have measured accretion rates by Donehew & Brittain (2011). Supplementing these results with accretion rates from Mendigutía et al. (2011), who used a similar methodology, and from Garcia Lopez et al. (2006), who based their



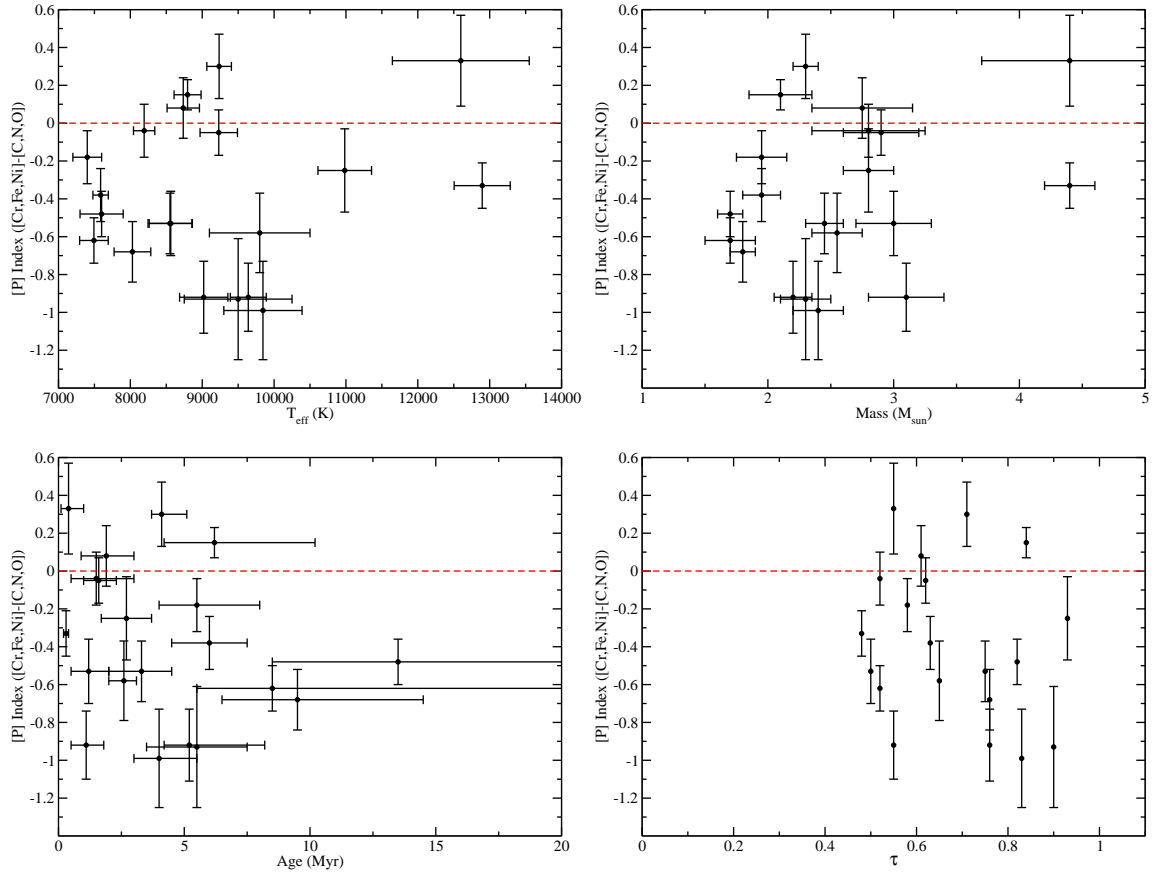


**Figure 3.** Trends in stellar parameters with the peculiarity index. The index is the average of Cr, Fe and Ni abundances each relative to solar, minus the average of the C, N and O abundances relative to solar. Plots are included for effective temperature, mass, age, and fractional pre-main sequence age ( $\tau$ ).

perfect, we find it does provide a reasonable approximation of the majority of the observed peculiarities in V380 Ori A.

Interestingly, HD 190073 and HD 101412 are both magnetic but do not show Ap/Bp chemical peculiarities. HD 190073 is chemically normal, while HD 101412 shows  $\lambda$  Boo type chemical peculiarities. Thus, unlike on the main sequence, not all pre-main sequence magnetic A and B stars are chemically peculiar. Atomic diffusion theory suggests that enough time must elapse after accretion and deep surface convection have halted for significant peculiarities to develop. The dissipation of a large convective envelope can be modelled easily enough, and in most models dissipates early in pre-main sequence life of A and B stars. However, determining when accretion has dropped sufficiently for atomic diffusion to dominate is much harder. Indeed it may depend on the circumstellar environment of the particular star, and thus not be reliably predictable.

The  $\lambda$  Boo peculiarities of HD 101412 presumably simply reflect the high incidence of  $\lambda$  Boo peculiarities in HAeBe stars in general. Thus, we suspect that these peculiarities are not a consequence of the magnetic field of HD 101412.

Modelling by Vick et al. (2011) suggests that HD 190073 has not yet had time to develop Ap/Bp chemical peculiarities. In their models, a star of this mass requires  $\sim 2$  Myr to develop peculiarities by atomic diffusion, while we find HD 190073 is only  $1.6^{+0.7}_{-0.6}$  Myr old. HD 101412 has almost

the same mass, and we find an age of only  $1.2^{+0.8}_{-0.7}$  Myr, thus by the models of Vick et al. (2011) it is also too young to have developed Ap/Bp peculiarities. The younger age of HD 101412 is consistent with the picture of its  $\lambda$  Boo type chemical peculiarities being due to selective accretion, since accretion is more likely to be ongoing earlier in a star's life.

It is interesting that the two stars in this sample with the largest amount of emission in their optical spectra are V380 Ori A and HD 190073, both of which are magnetic. In particular, the emission mostly appears in lines that would be strongly in absorption for a purely photospheric spectrum of the star. HD 101412, the third magnetic star, displays a fairly modest amount of emission. Additionally, the measured accretion rates for V380 Ori and HD 190073 are both substantially higher than for other stars in our sample ( $\log \dot{M}_{acc} = -5.6 [M_{\odot} \text{ yr}^{-1}]$  for V380 Ori,  $\log \dot{M}_{acc} = -5.0 [M_{\odot} \text{ yr}^{-1}]$  for HD 190073; Donehew & Brittain 2011; Mendigutia et al. 2011). The impact of the secondary in V380 Ori does not appear to be considered in the measurement of the star's accretion rate, and thus it may be somewhat inaccurate. In classical T Tauri stars, the strong emission in their spectra is thought to result from magnetically channelled accretion flows falling onto the star. We speculate that the strong emission in V380 Ori A and HD 190073 might be produced by a similar process. However, it is not clear whether this is the case, both because of the

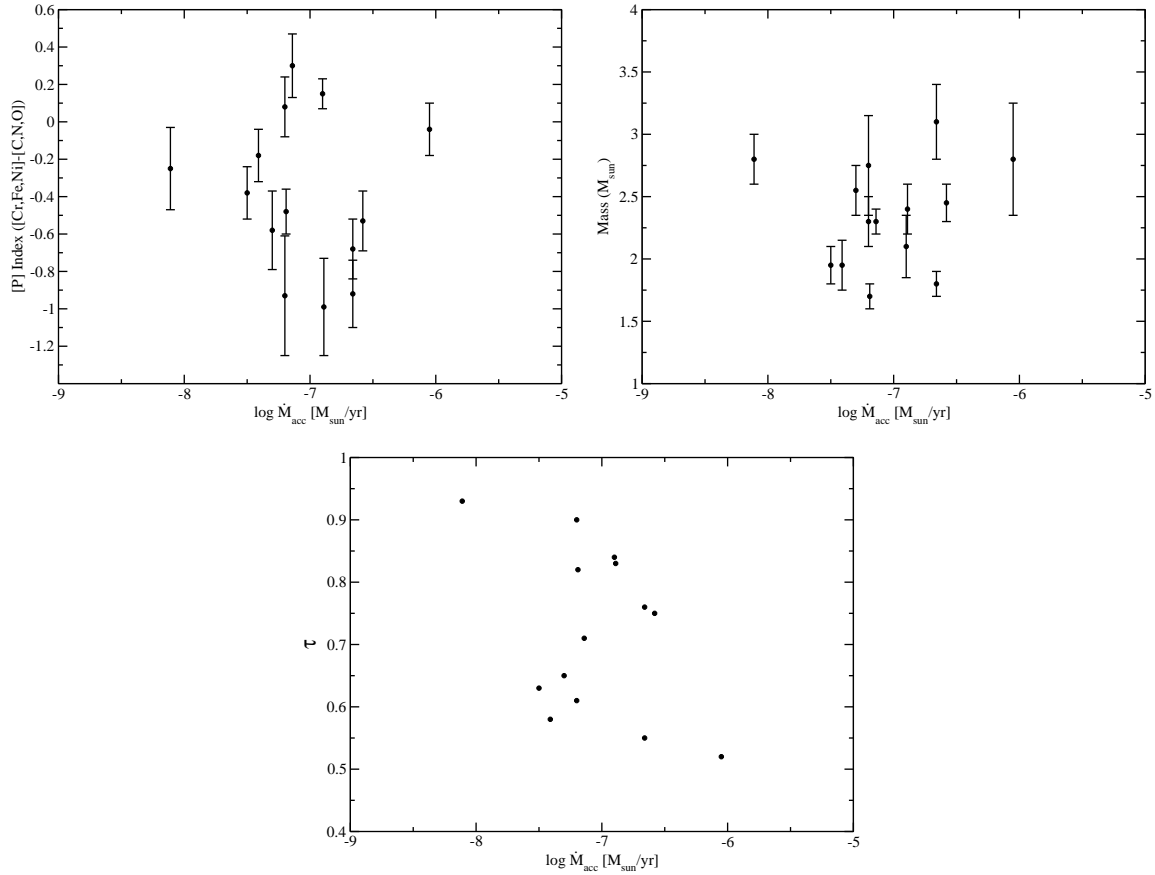


**Figure 4.** Trends in stellar parameters with literature accretion rates. Plots are included for our chemical peculiarity index, stellar mass, and fractional pre-main sequence age ( $\tau$ ).

small sample size, and because the non-magnetic stars in the sample are biased towards lower emission stars (since large amounts of emission limit the abundance analysis). Magnetic fields are not detected in individual emission lines for any of our stars, thus we cannot use those lines to assess the presence of magnetospheric accretion directly.

The three stars in our sample with confirmed magnetic fields also have the lowest  $v \sin i$  values (for more analysis see Alecian et al. 2012b). In this respect these three magnetic HAeBe stars are similar to Ap/Bp stars, which rotate slower than normal non-magnetic A and B stars. The low  $v \sin i$  of the magnetic HAeBe stars HD 200775A ( $v \sin i = 26 \pm 2 \text{ km s}^{-1}$ , Alecian et al. 2008a) and of NGC 2244 OI 201 ( $v \sin i = 23.5 \pm 0.5 \text{ km s}^{-1}$ , Alecian et al. 2008b), and the moderate  $v \sin i$  of HD 72106 A ( $v \sin i = 41.0 \pm 0.6 \text{ km s}^{-1}$ , Folsom et al. 2008) support this observation. However, the very high  $v \sin i$  of NGC 6611 W610 ( $v \sin i = 190 \pm 10 \text{ km s}^{-1}$ , Alecian et al. 2008b) indicates that not all magnetic HAeBe stars rotate slowly. Nevertheless, the large number of low  $v \sin i$  magnetic HAeBe stars suggests that magnetic braking may have occurred in many of these stars (see Alecian et al. 2012b).

Several other very young magnetic A and B stars are known to have chemical peculiarities. Folsom et al. (2008) examined the magnetic star HD 72106 A, and found Ap/Bp peculiarities. They find that the star has a mass of  $2.4 M_{\odot}$ . While they were unable to firmly conclude that HD 72106 A

is on the pre-main sequence, they do find that the system is between 6 and 13 Myr from the birthline, based on the H-R diagram position of the secondary in the binary system. The pattern of abundances seen in HD 72106 A is similar to that seen in V380 Ori A, but more extreme. Overabundances of iron peak elements and a weak overabundance of Si is seen in both stars. However, the strong He underabundance seen in HD 72106 A is not seen in V380 Ori A. The differences in abundances between the stars could be due to V380 Ori A being hotter and more massive HD 72106 A, or due to HD 72106 A being more evolved.

Bagnulo et al. (2004) investigated the main sequence magnetic star NGC 2244-334, which is a member of the open cluster NGC 2244, and found Ap/Bp peculiarities. They found that the star has a mass of  $\sim 4 M_{\odot}$  and commented that, as a cluster member, the star is likely  $\sim 2$  Myr old as measured from the ZAMS. This is a similar mass to V380 Ori A, though NGC 2244-334 is somewhat older. The peculiarities they found are very similar to those of HD 72106 A, with overabundances in iron peak elements of 1-2 dex, a somewhat weaker overabundance of Si, and a strongly underabundant He. This is again similar to what we see in V380 Ori A, though much stronger, and with a He underabundance.

Alecian et al. (2008b) studied the magnetic Herbig Be star NGC 6611 W601, and noted peculiarly strong He and Si lines in its spectrum. This suggest the star likely represents a

pre-main sequence He-strong star, but a detailed abundance analysis has yet to be performed. While this pattern of peculiarities would be different from that of V380 Ori A, the star has a much higher temperature of  $22500 \pm 2500$  K and a much higher mass of  $10.2^{+1.2}_{-0.7} M_{\odot}$  (Alecian et al. 2008b). For a main sequence magnetic star in this temperature and mass range, one would expect to see He-strong peculiarities, rather than Ap/Bp peculiarities. Alecian et al. (2008b) estimate the age of NGC 6611 W601 to be less than 0.06 Myr from the birthline of Palla & Stahler (1993, for an accretion rate of  $10^{-4} M_{\odot} \text{ yr}^{-1}$ ), based on its H-R diagram position. While this is very young, there are no models from Vick et al. (2011) for a comparable mass. We do note, however, that Vick et al. (2011) find peculiarities developing faster for more massive models.

Thus, while the peculiarities seen in V380 Ori A are weak, the pattern of peculiarities is consistent with those seen in other young intermediate mass magnetic stars. This is consistent with the hypothesis that the weak peculiarities we see in this star will develop into the stronger peculiarities seen in most main sequence Ap/Bp stars.

### 6.3 Chemically normal stars

We find no hints of any chemical peculiarities in the stars of our sample other than  $\lambda$  Boo peculiarities and the weak Bp peculiarities in V380 Ori A. Thus we find no evidence for Am or HgMn stars on the pre-main sequence. Our sample is not large enough to definitively exclude the existence of Am and HgMn stars at the same incidence as on the main sequence. However, if the roughly 10-20% incidence (e.g. Smith 1996) of these stars on the main sequence is extended to the pre-main sequence, we would expect to have seen two to four such stars. Thus it is possible that these peculiarities do not form on the pre-main sequence, unlike for Ap/Bp stars. The atomic diffusion thought to give rise to these peculiarities may be disrupted by weak accretion more readily than the diffusion in the presence of a magnetic field that produces Ap/Bp stars. The presence of a magnetic field may stabilise a stellar atmosphere and increase diffusion velocities, potentially making diffusion in the presence of a magnetic field more robust (Michaud 1970; Michaud et al. 1981). Alternately, diffusion in non-magnetic stars may simply require more time than the pre-main sequence lifetime of these stars to produce significant peculiarities.

The large majority of young A and B stars analysed, both on the main sequence and on the pre-main sequence (e.g. Acke & Waelkens 2004), have been found to be chemically normal. A very precise study of A and B star abundances by Fossati et al. (2009) investigated what ‘normal’ abundances are for A and B stars. They found that solar abundances are a good approximation, though there were small deviations for specific elements, which appeared to depend on the temperature of the star. Studies of nearby open clusters support this conclusion (e.g. Fossati et al. 2008; Villanova et al. 2009; Fossati et al. 2011).

Acke & Waelkens (2004) performed an abundance analysis of 24 pre-main sequence and very young main sequence stars, based on equivalent widths. A comparison of individual results for the 7 stars we have in common with their study is discussed in Sect. A. Our results are generally consistent, although we are able to determine abundances for

a wider range of elements, and in many cases provide more precise abundances. The one notable difference in our results is for HD 139614. For this star our more accurate  $T_{\text{eff}}$  allows us to classify the star as  $\lambda$  Boo, while Acke & Waelkens (2004) could only comment that it appeared to be metal weak. In total Acke & Waelkens (2004) found only one Herbig star that was also a clear  $\lambda$  Boo star (HD 100546), and they noted that AB Aur shows hints of  $\lambda$  Boo peculiarity. In part this difference in detection rates may due to our more accurate  $T_{\text{eff}}$  and  $\log g$  values, as the case of HD 139614 demonstrates. Our higher precision, due to an improved methodology and higher S/N observations, is also a significant part of this difference. Finally, both our studies deal with a fairly small number of stars, and thus the true incidence of  $\lambda$  Boo peculiarities in HAeBe stars remains somewhat uncertain.

### 6.4 Possible Veiling

One concern when analysing spectra of T Tauri stars is veiling. Veiling is additional continuum emission, usually from an accretion shock (or other circumstellar material), which makes spectral lines appear weaker than they would in a purely photospheric spectrum. In HAeBe stars, veiling can be seen in the UV (e.g. Donehew & Brittain 2011), but usually is considered to be unimportant in the optical (e.g. Böhm & Catala 1993; Hernández et al. 2004; Cowley et al. 2010; Donehew & Brittain 2011). HAeBe stars are intrinsically much more luminous than T Tauri stars, thus much more emission from an accretion shock would be needed to have the same veiling effect. Measured accretion rates for HAeBe stars are usually not much larger than for T Tauri stars, thus it is unlikely that HAeBe stars would have much larger amounts of emission from accretion shocks. Consequently, we would not expect veiling to have much impact on HAeBe star spectra.

If veiling is present in our observations it could make a star appear to be metal poor when it is not, thus it is important to check for veiling. If it is present in our spectra, veiling should have some wavelength dependence. We have compared abundances derived from different wavelength regions for individual stars. No clear correlation of abundance with wavelength was found, suggesting that veiling is unimportant in these stars. Veiling should affect all lines in a wavelength region similarly. Thus, if it is present veiling should affect most elements similarly, since the lines for most elements are widely distributed in our spectra. In particular, it could not produce underabundances in iron peak elements while keeping solar abundances of C and O that we see in many of the stars in our sample. Therefore veiling should not affect the *relative* abundances of C, N, and O to Fe, even if it were present at a significant level in our spectra. We conclude it is unlikely that veiling has a significant impact on our derived abundances, and even if veiling is present it is not obvious how it could produce peculiar abundance patterns.

Arguably, the pattern of  $\lambda$  Boo underabundances we observe could be due to weak emission infilling in all the lines of some elements, however this is very unlikely. We have searched carefully for emission in lines, both by looking for unexpected variability and by looking for lines with shapes inconsistent with rotational broadening. Thus we have ex-

cluded most if not all lines with emission. More importantly, lines of an element with lower excitation potentials are more likely to have stronger emission, thus emission would not be uniform across all lines. If emission infilling was occurring and otherwise undetected, we would observe it as an inability to simultaneously fit a wide range of lines of one element with one abundance. We do not find this, and consequently can safely conclude that the  $\lambda$  Boo peculiarities we detect are real, and not simply due to emission infilling.

## 7 CONCLUSIONS

We have performed a detailed abundance analysis of 21 stars, 20 of which are Herbig Ae and Be stars, 1 of which ( $\pi$  Cet) is not a Herbig star, but may still be on the pre-main sequence. Three of these stars have confirmed magnetic fields, while magnetic fields do not appear to be present at detectable levels in the remaining 18.

We find 9 stars that are chemically normal (one of which is rather uncertain), 11 that show  $\lambda$  Boötis chemical peculiarities, and one that is weakly Ap/Bp. This is a remarkably large fraction of stars that display  $\lambda$  Boo type peculiarities. On the main sequence, only  $\sim 2\%$  of stars display  $\lambda$  Boo peculiarities (Paunzen 2001). We interpret this as evidence in favour of a selective accretion hypothesis for the development of  $\lambda$  Boo peculiarities. Since Herbig stars are either accreting or have recently finished accreting, a process which depends on accretion should be seen more frequently in these stars.

Of the three magnetic stars, HD 101412 displays  $\lambda$  Boo peculiarities, HD 190073 is chemically normal, and V380 Ori is weakly Bp. Thus it appears that magnetic Herbig stars can display Ap/Bp type peculiarities, but not all magnetic Herbig stars do. This is in contrast to main sequence magnetic A and late B stars, which always display Ap/Bp type peculiarities (Aurière et al. 2007). The presence of  $\lambda$  Boo peculiarities in a magnetic star appears to simply reflect the high incidence of these peculiarities in all Herbig stars.

## ACKNOWLEDGEMENTS

GAW and JDL are supported by Natural Science and Engineering Research Council (NSERC Canada) Discovery Grants, and GAW is supported by a Department of National Defence (Canada) ARP grant.

## REFERENCES

- Abt H. A., Morrell N. I., 1995, *ApJS*, 99, 135  
 Acke B., Waelkens C., 2004, *A&A*, 427, 1009  
 Alecian E., Catala C., Wade G. A., Donati J.-F., Petit P., Landstreet J. D., Böhm T., Bouret J.-C., Bagnulo S., Folsom C., Grunhut J., Silvester J., 2008a, *MNRAS*, 385, 391  
 Alecian E., Wade G. A., Catala C., Bagnulo S., Boehm T., Bohlender D., Bouret J.-C., Donati J.-F., Folsom C. P., Grunhut J., Landstreet J. D., 2008b, *A&A*, 481, L99  
 Alecian E., Wade G. A., Catala C., Bagnulo S., Böhm T., Bouret J., Donati J., Folsom C. P., Grunhut J., Landstreet J. D., 2009, *MNRAS*, 400, 354  
 Alecian E., Wade G. A., Catala C., Grunhut J. H., Boehm T., Bouret J.-C., Flood J., Folsom C. P., Landstreet J. D., Marsden S. C., Waite I. A., 2012a, *MNRAS*, submitted  
 Alecian E., Wade G. A., Catala C., Grunhut J. H., Landstreet J. D., Boehm T., Bouret J.-C., Flood J., Folsom C. P., 2012b, *MNRAS*, submitted  
 Andrievsky S. M., Chernyshova I. V., Paunzen E., Weiss W. W., Korotin S. A., Beletsky Y. V., Handler G., Heiter U., Korotina L., Stütz C., Weber M., 2002, *A&A*, 396, 641  
 Andrievsky S. M., Paunzen E., 2000, *MNRAS*, 313, 547  
 Aurière M., Wade G. A., Silvester J., Lignières F., Bagnulo S., Bale K., Dintrans B., Donati J. F., et al. 2007, *A&A*, 475, 1053  
 Bagnulo S., Hensberge H., Landstreet J. D., Szeifert T., Wade G. A., 2004, *A&A*, 416, 1149  
 Bagnulo S., Landstreet J. D., Fossati L., Kochukhov O., 2011, *A&A*, submitted  
 Balona L. A., 1994, *MNRAS*, 268, 119  
 Behrend R., Maeder A., 2001, *A&A*, 373, 190  
 Bohlender D. A., Landstreet J. D., 1990, *MNRAS*, 247, 606  
 Böhm T., Catala C., 1993, *A&AS*, 101, 629  
 Brown A. G. A., de Geus E. J., de Zeeuw P. T., 1994, *A&A*, 289, 101  
 Catala C., Alecian E., Donati J.-F., Wade G. A., Landstreet J. D., Böhm T., Bouret J.-C., Bagnulo S., Folsom C., Silvester J., 2007, *A&A*, 462, 293  
 Charbonneau P., 1993, *ApJ*, 405, 720  
 Cowley C. R., Hubrig S., González J. F., Savanov I., 2010, *A&A*, 523, A65  
 de Winter D., van den Ancker M. E., Maira A., Thé P. S., Djie H. R. E. T. A., Redondo I., Eiroa C., Molster F. J., 2001, *A&A*, 380, 609  
 de Zeeuw P. T., Hoogerwerf R., de Bruijne J. H. J., Brown A. G. A., Blaauw A., 1999, *AJ*, 117, 354  
 Dolan C. J., Mathieu R. D., 2001, *AJ*, 121, 2124  
 Donati J.-F., Collier Cameron A., Semel M., Hussain G. A. J., Petit P., Carter B. D., Marsden S. C., Mengel M., López Ariste A., Jeffers S. V., Rees D. E., 2003, *MNRAS*, 345, 1145  
 Donati J.-F., Semel M., Carter B. D., Rees D. E., Collier Cameron A., 1997, *MNRAS*, 291, 658  
 Donehew B., Brittain S., 2011, *AJ*, 141, 46  
 ESA, 1997, *The Hipparcos and Tycho Catalogues*, ESA SP-1200  
 Faraggiana R., Bonifacio P., 2005, *A&A*, 436, 697  
 Folsom C. P., Wade G. A., Kochukhov O., Alecian E., Catala C., Bagnulo S., Böhm T., Bouret J., Donati J., Grunhut J., Hanes D. A., Landstreet J. D., 2008, *MNRAS*, 391, 901  
 Fossati L., Bagnulo S., Landstreet J., Wade G., Kochukhov O., Monier R., Weiss W., Gebran M., 2008, *A&A*, 483, 891  
 Fossati L., Folsom C. P., Bagnulo S., Grunhut J. H., Kochukhov O., Landstreet J. D., Paladini C., Wade G. A., 2011, *MNRAS*, 413, 1132  
 Fossati L., Ryabchikova T., Bagnulo S., Alecian E., Grunhut J., Kochukhov O., Wade G., 2009, *A&A*, 503, 945  
 Garcia Lopez R., Natta A., Testi L., Habart E., 2006, *A&A*, 459, 837  
 Grevesse N., Asplund M., Sauval A. J., 2005, in Alecian G., Richard O., Vauclair S., eds, *Element Stratification in Stars: 40 Years of Atomic Diffusion* Vol. 17 of EAS Pub. Ser., The New Solar Chemical Composition. p. 21

- Guimarães M. M., Alencar S. H. P., Corradi W. J. B., Vieira S. L. A., 2006, *A&A*, 457, 581
- Heiter U., 2002, *A&A*, 381, 959
- Herbst W., Shevchenko V. S., 1999, *AJ*, 118, 1043
- Hernández J., Calvet N., Briceño C., Hartmann L., Berlind P., 2004, *AJ*, 127, 1682
- Hubrig S., Mikulášek Z., González J. F., Schöller M., Ilyin I., Curé M., Zejda M., Cowley C. R., Elkin V. G., Pogodin M. A., Yudin R. V., 2011, *A&A*, 525, L4
- Hubrig S., Pogodin M. A., Yudin R. V., Schöller M., Schnerr R. S., 2007, *A&A*, 463, 1039
- Hubrig S., Schöller M., Yudin R. V., 2004, *A&A*, 428, L1
- Hubrig S., Stelzer B., Schöller M., Grady C., Schütz O., Pogodin M. A., Curé M., Hamaguchi K., Yudin R. V., 2009, *A&A*, 502, 283
- Hubrig S., Yudin R. V., Schöller M., Pogodin M. A., 2006, *A&A*, 446, 1089
- Kamp I., Paunzen E., 2002, *MNRAS*, 335, L45
- Kenyon S. J., Hartmann L., 1995, *ApJS*, 101, 117
- Kochukhov O. P., 2007, in I. I. Romanyuk, D. O. Kudryavtsev, O. M. Neizvestnaya, & V. M. Shapoval ed., *Physics of Magnetic Stars Spectrum synthesis for magnetic, chemically stratified stellar atmospheres*. pp 109–118
- Kupka F., Piskunov N., Ryabchikova T. A., Stempels H. C., Weiss W. W., 1999, *A&AS*, 138, 119
- Kurucz R., 1993, *CDROM Model Distribution*, Smithsonian Astrophys. Obs.
- Landstreet J. D., 1988, *ApJ*, 326, 967
- Leinert C., Richichi A., Haas M., 1997, *A&A*, 318, 472
- Malfait K., Bogaert E., Waelkens C., 1998, *A&A*, 331, 211
- Marsden S. C., Jardine M. M., Ramírez Vélez J. C., Alecian E., Brown C. J., Carter B. D., Donati J.-F., Dunstone N., Hart R., Semel M., Waite I. A., 2011, *MNRAS*, 413, 1922
- Mendigutía I., Calvet N., Montesinos B., Mora A., Muzerolle J., Eiroa C., Oudmaijer R. D., Merín B., 2011, *A&A*, 535, A99
- Michaud G., 1970, *ApJ*, 160, 641
- Michaud G., Charland Y., 1986, *ApJ*, 311, 326
- Michaud G., Charland Y., Megessier C., 1981, *A&A*, 103, 244
- Miroshnichenko A. S., Bjorkman K. S., Chentsov E. L., Klochkova V. G., Gray R. O., García-Lario P., Perea Calderón J. V., 2001, *A&A*, 377, 854
- Morel P., 1997, *A&AS*, 124, 597
- Muzerolle J., D'Alessio P., Calvet N., Hartmann L., 2004, *ApJ*, 617, 406
- Palla F., Stahler S. W., 1993, *ApJ*, 418, 414
- Paunzen E., 2001, *A&A*, 373, 633
- Paunzen E., Iliev I. K., Kamp I., Barzova I. S., 2002, *MNRAS*, 336, 1030
- Press W. H., Teukolsky S. A., Vetterling W. T., Flannery B. P., 1992, *Numerical Recipes in FORTRAN*, 2nd edn. Cambridge University Press, Cambridge
- Ripepi V., Bernabei S., Marconi M., Palla F., et al. 2006, *A&A*, 449, 335
- Semel M., Donati J.-F., Rees D. E., 1993, *A&A*, 278, 231
- Smith K. C., 1996, *Ap&SS*, 237, 77
- Stütz C., Paunzen E., 2006, *A&A*, 458, L17
- Sylvester R. J., Skinner C. J., Barlow M. J., Mannings V., 1996, *MNRAS*, 279, 915
- Turcotte S., 2002, *ApJ*, 573, L129
- Turcotte S., Charbonneau P., 1993, *ApJ*, 413, 376
- van Leeuwen F., 2007, *A&A*, 474, 653
- Venn K. A., Lambert D. L., 1990, *ApJ*, 363, 234
- Vick M., Michaud G., Richer J., Richard O., 2011, *A&A*, 526, A37
- Vieira S. L. A., Corradi W. J. B., Alencar S. H. P., Mendes L. T. S., Torres C. A. O., Quast G. R., Guimarães M. M., da Silva L., 2003, *AJ*, 126, 2971
- Villanova S., Carraro G., Saviane I., 2009, *A&A*, 504, 845
- Wade G. A., Bagnulo S., Drouin D., Landstreet J. D., Monin D., 2007, *MNRAS*, 376, 1145
- Wade G. A., Bagnulo S., Kochukhov O., Landstreet J. D., Piskunov N., Stift M. J., 2001, *A&A*, 374, 265
- Wade G. A., Drouin D., Bagnulo S., Landstreet J. D., Mason E., Silvester J., Alecian E., Böhm T., Bouret J.-C., Catala C., Donati J.-F., 2005, *A&A*, 442, L31
- Waters L. B. F. M., Trams N. R., Waelkens C., 1992, *A&A*, 262, L37

## APPENDIX A: RESULTS FOR INDIVIDUAL STARS

### Non-magnetic stars

#### A1 $\pi$ Cet (HD 17081)

$\pi$  Cet (HD 17081) is a cool B star that was studied in detail by Fossati et al. (2009). They performed a very precise, detailed abundance analysis, and considered the star to be a good example of a ‘normal’ cool B star.  $\pi$  Cet is not a Herbig Be star by the strict definition, since it has no strong emission in its optical spectrum. However, the star does display an infrared excess (Malfait et al. 1998), as well as some unexplained line profile variations (Fossati et al. 2009), and an H-R diagram position to the right of the main sequence. Thus the star is certainly very young, and possibly still on the pre-main sequence, despite the lack of clear emission. Based on the H-R diagram position of the star, it appears to be less than 0.5 Myr from the birth line, and almost certainly is less than 1 Myr old. Malfait et al. (1998) suggested this star was a Vega-type star, a classification which is consistent with our observations.

In order to check the accuracy of our methodology, we analysed an observation of  $\pi$  Cet and compared our results with the results of Fossati et al. (2009). Our results are completely consistent with those of Fossati et al. (2009), for temperature, gravity,  $v \sin i$ , and abundances. Our atmospheric parameters and abundances are compared with those of Fossati et al. (2009) in Table A1, and the differences between our abundances and those of Fossati et al. (2009) are plotted in Fig. A1. The excellent agreement between our results and Fossati et al. (2009) demonstrates the accuracy of our methodology.

$\pi$  Cet was observed spectropolarimetricly by Wade et al. (2007), who did not detect a magnetic field. Alecian et al. (2012a) also found no magnetic field in  $\pi$  Cet, and thus we consider the star to be non-magnetic.

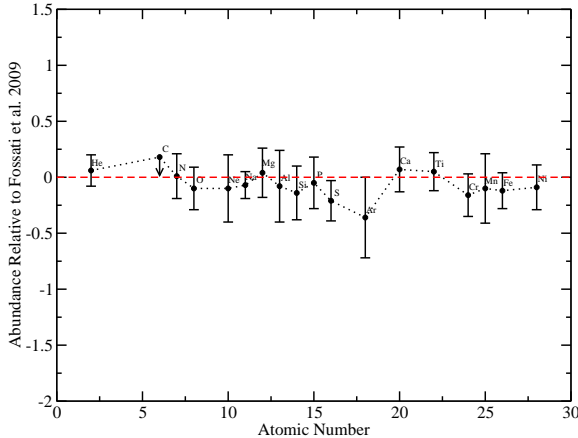


**Figure A1.** The difference between our final abundances and those of Fossati et al. (2009) for  $\pi$  Cet. A good agreement between the two sets of abundances is found.

**Table A1.** Our results compared with those of Fossati et al. (2009) for  $\pi$  Cet.

	Fossati et al. (2009)	This work
$T_{\text{eff}}$ (K)	$12800 \pm 200$	$12900 \pm 400$
$\log g$	$3.75 \pm 0.1$	$3.8 \pm 0.2$
$v \sin i$ ( $\text{km s}^{-1}$ )	$20.2 \pm 0.9$	$20.9 \pm 1.2$
$\xi$ ( $\text{km s}^{-1}$ )	$1.0 \pm 0.5$	$1.7 \pm 1.0$
He	$-0.97 \pm 0.04$	$-0.91 \pm 0.14$
C	$-3.58 \pm 0.07$	$\leq -3.4$
N	$-4.03 \pm 0.13$	$-4.03 \pm 0.15$
O	$-3.06 \pm 0.14$	$-3.16 \pm 0.13$
Ne	$-3.66 \pm 0.09$	$-3.76 \pm 0.28$
Na	$-5.23 \pm 0.07$	$-5.3 \pm 0.1$
Mg	$-4.47 \pm 0.16$	$-4.43 \pm 0.15$
Al	$-5.73 \pm 0.27$	$-5.81 \pm 0.17$
Si	$-4.41 \pm 0.2$	$-4.55 \pm 0.14$
P	$-6.38 \pm 0.19$	$-6.43 \pm 0.14$
S	$-4.78 \pm 0.16$	$-4.99 \pm 0.08$
Ar	$-5.24 \pm 0.19$	$-5.6 \pm 0.3$
Ca	$-5.77$	$-5.7 \pm 0.2$
Ti	$-7.42 \pm 0.08$	$-7.37 \pm 0.15$
Cr	$-6.41 \pm 0.1$	$-6.57 \pm 0.16$
Mn	$-6.5 \pm 0.09$	$-6.6 \pm 0.3$
Fe	$-4.58 \pm 0.14$	$-4.70 \pm 0.08$
Ni	$-5.76 \pm 0.19$	$-5.85 \pm 0.06$

## A2 HD 31293 (AB Aur)

We derive  $T_{\text{eff}} = 9800 \pm 700$  K and  $\log g = 3.9 \pm 0.3$  for HD 31293 (AB Aur). This  $T_{\text{eff}}$  is consistent with Acke & Waelkens (2004), but our  $\log g$  is inconsistent with their (remarkably high) value of 5.0. The  $T_{\text{eff}}$  and  $\log g$  are both consistent with Böhm & Catala (1993). We find solar He and O abundances, C and N are  $1\sigma$  above solar, while the iron peak elements are consistently  $1\sigma$  below solar. The systematic underabundance of iron peak elements by  $\sim 0.3$  dex suggests the star may be a weak  $\lambda$  Boo star. This is strengthened somewhat by the observation that the iron peak elements are

$\sim 0.5$  dex below the average C, N, and O abundance. Based on these underabundances, we conclude that the star most likely is a weak  $\lambda$  Boo star, but it is a marginal case.

Acke & Waelkens (2004) derive abundances for O, N, and Si that are consistent with ours, but their Fe abundance of 1 dex below solar (based on 2 Fe I lines) is inconsistent with our value. This difference may be due to the higher  $\log g$  Acke & Waelkens (2004) used. Alternately, it is possible their measurement was impacted by the large amount of emission in the spectrum of HD 31293. Both Fe abundances are consistent with a  $\lambda$  Boo classification of the star, but we prefer our larger abundance since it is based on larger number and a wider range of lines, and it is consistent with the neighbouring iron peak element abundances we derive.

Alecian et al. (2012a) find no magnetic field in HD 31293. Wade et al. (2007) also find no magnetic field in this star, thus we consider it to be non-magnetic.

## A3 HD 31648

For HD 31648 we derive an  $T_{\text{eff}}$  of  $8800 \pm 190$  K and a  $\log g$  of  $4.1 \pm 0.2$ , which is consistent with Acke & Waelkens (2004). We find most abundances within  $1\sigma$  of solar, and all abundances except Mg and Ti within  $2\sigma$ . The abundances are systematically slightly above solar and may reflect a slightly enhanced metallicity, or a slightly overestimated  $T_{\text{eff}}$ .

Our Ca and Fe abundances are consistent with Acke & Waelkens (2004), our C abundance is consistent at  $2\sigma$ , as is our Y abundance if we assume the uncertainty on their value is comparable to ours. Our Si and Mg abundances are not consistent with Acke & Waelkens (2004), although their abundances are based on only 1 line and thus are likely uncertain. The large  $v \sin i$  of this star causes significant blending in its spectrum. This could explain the discrepancies between our results, since the Acke & Waelkens (2004) abundances are based on equivalent width measurements, which can easily be influenced by unaccounted-for blending.

HD 31648 was not found to have a magnetic field by Alecian et al. (2012a). No magnetic field was found by Wade et al. (2007) either. Hubrig et al. (2006) claimed a weak detection of a magnetic field in their observation of HD 31648 but, in the re-reduction of the observation made by Hubrig et al. (2007) the field is below their detection threshold. Surprisingly, Hubrig et al. (2007) report a signal the  $H\beta$ ,  $H\gamma$ ,  $H\delta$ , and Ca H & K lines of their  $V/I$  spectrum, which they interpret as a “circumstellar” magnetic field. This result has yet to be independently confirmed. A careful examination of the  $H\beta$ ,  $H\gamma$ ,  $H\delta$ , and Ca H & K lines in our spectra shows no polarisation signature. Bagnulo et al. (2011) re-reduced a wide range of spectropolarimetric observations from the FORS1 instrument at the VLT, including the observations of Hubrig et al. (2006). They find no evidence for a magnetic field in HD 31648. Considering the lack of evidence for a photospheric magnetic field, and the absence of a confirmation of a “circumstellar” magnetic field, we conclude that HD 31648 is non-magnetic.

## A4 HD 36112

For HD 36112 we find  $T_{\text{eff}} = 8190 \pm 150$  K and  $\log g = 4.1 \pm 0.4$ , both of which are somewhat greater than the

$T_{\text{eff}} = 7750$  and  $\log g = 3.5$  of Acke & Waelkens (2004). Our uncertainty on  $T_{\text{eff}}$  may be overly optimistic, though it does reflect the scatter in  $T_{\text{eff}}$  derived from different spectral windows. The uncertainties on the calibration of  $T_{\text{eff}}$  become important at this level, and thus there may be some systematic uncertainty not included in our error bar. Most of our derived abundances are within  $1\sigma$  of solar, and all are within  $2\sigma$ . There are no systematic enhancements or depletions, thus we conclude HD 36112 is chemically normal, with solar abundances.

Our abundances are consistent with those of Acke & Waelkens (2004) for C, Si, S, Ca, Sc, Cr, Mn, Fe, and Ni. Our abundance for Ti and Y differ by  $\sim 2\sigma$ . These differences may be a consequence of our hotter temperature, or they may be due to the small number of lines Acke & Waelkens (2004) used for determining those abundances.

Alecian et al. (2012a) do not detect a magnetic field in this star. In their FORS1 observations Wade et al. (2007) do not detect a magnetic field, nor do Bagnulo et al. (2011) in their re-reduction of the FORS1 observations.

#### A5 HD 68695

For HD 68695 we derive  $T_{\text{eff}} = 9000 \pm 300$  K and  $\log g = 4.3 \pm 0.3$ . We find C, N, O, and S abundances that are  $\sim 1\sigma$  above solar, while iron peak abundances are 2 to  $3\sigma$  below solar ( $\sim 0.7$  dex below solar), except for the rather uncertain Mn abundance. We conclude that this star has clear  $\lambda$  Boo peculiarities.

No magnetic field was detected in HD 68695 by either Alecian et al. (2012a) or by Wade et al. (2007), thus we consider the star to be non-magnetic.

#### A6 HD 139614

HD 139614 was analysed by Acke & Waelkens (2004) using an  $T_{\text{eff}}$  of 8000 K. They found an overall deficiency of metals, but no clear evidence of the selective depletion characteristic of  $\lambda$  Boo stars. We find HD 139614 to have an  $T_{\text{eff}}$  of  $7600 \pm 300$  K, and a  $\log g$  of  $3.9 \pm 0.3$ , which is consistent with the results of  $T_{\text{eff}} = 7400 \pm 200$  K and  $\log g = 4.0 \pm 0.4$  reported by Guimarães et al. (2006), and marginally consistent with Acke & Waelkens (2004) (at  $1.3\sigma$  in  $T_{\text{eff}}$  and  $2\sigma$  in  $\log g$ ). We consider our parameters (and Guimarães et al. 2006) to be more accurate, since Acke & Waelkens (2004) values were based on the spectral classification of Malfait et al. (1998), which could be influenced by chemical peculiarities in the star. In fact, for our parameters we find a clear  $\lambda$  Boo pattern of abundances, with solar C, N, and O, and underabundant iron peak elements.

No magnetic field was detected in HD 139614 by Alecian et al. (2012a). Hubrig et al. (2004) claimed a detection of a magnetic field in this star, which was not supported by Wade et al. (2005). Further observations by Hubrig et al. (2009) did not detect a magnetic field in the star, though they comment on a possible signal in the Ca H and K lines. In their re-reduction of FORS data, Bagnulo et al. (2011) find no evidence for a magnetic field in HD 139614, and conclude that the reported detection by Hubrig et al. (2004) is likely spurious. Consequently, we consider HD 139614 not to have a significant magnetic field.

#### A7 HD 141569

We find  $T_{\text{eff}} = 9800 \pm 500$  K and  $\log g = 4.2 \pm 0.4$  for HD 141569, which is consistent with the parameters found by Guimarães et al. (2006). We find  $\lambda$  Boo peculiarities in this star, with solar He, C and N, possibly overabundant O, and underabundant iron peak elements.

Alecian et al. (2012a) do not detect a magnetic field in the star. Wade et al. (2007) also find no magnetic field, thus we conclude HD 141569 does not have a significant magnetic field.

#### A8 HD 142666

For HD 142666 we find  $T_{\text{eff}} = 7500 \pm 200$  K and  $\log g = 3.9 \pm 0.3$ , which is consistent with Guimarães et al. (2006). We find weak  $\lambda$  Boo peculiarities in this star. C, O, Na and S have solar abundance, while the iron peak elements are consistently  $\sim 0.5$  dex below solar, except for the rather uncertain Co abundance.

Wade et al. (2007) observed the star and found no magnetic field. Alecian et al. (2012a) find no magnetic field in the star either.

#### A9 HD 144432

For HD 144432 we find  $T_{\text{eff}} = 7400 \pm 200$  K and  $\log g = 3.9 \pm 0.3$ , which is consistent with Guimarães et al. (2006). The abundances of all elements we derive are within  $2\sigma$  of solar, and most are within  $1\sigma$ . There are no clear trends in abundances of different elements, thus we consider the star chemically normal, with nearly solar metallicity.

Alecian et al. (2012a) observed HD 144432 twice and found no magnetic field. Wade et al. (2007) also found no magnetic field in the star. Hubrig et al. (2007) claim a weak magnetic field detection in this star in one observation, but Hubrig et al. (2004) and Hubrig et al. (2009) did not detect a significant magnetic field in the star. Bagnulo et al. (2011) re-reduced the one observation of HD 144432 with a magnetic field detection from Hubrig et al. (2007). Bagnulo et al. (2011) do find a magnetic field in the observation at a  $4.9\sigma$  level ( $\langle B_z \rangle = -108 \pm 22$  G). However, they caution that the impact of instrumental effects on the detection of weak magnetic fields is not well understood for the FORS1 instrument. They conclude that for weak magnetic fields, detections at less than  $6\sigma$  should not be considered definite, and require supporting observations. Thus, while we cannot completely exclude the possibility of a magnetic field in HD 144432, based on the large majority of the evidence (five out of six observations) we conclude that HD 144432 likely has no significant magnetic field.

#### A10 HD 163296

We determine an  $T_{\text{eff}}$  of  $9200 \pm 300$  K and a  $\log g$  of  $4.2 \pm 0.3$ , which is consistent with Guimarães et al. (2006). We find the abundances of most elements to be within uncertainty of solar, though Mg and Cr are both overabundant at slightly more than  $2\sigma$ . With largely solar abundance and no clear selective depletion or enhancement, we conclude that the star is chemically normal.

Alecian et al. (2012a) do not find a magnetic field in HD 163296. Hubrig et al. (2009) also do not detect a magnetic field in the star, thus we conclude the star is non-magnetic

#### A11 HD 169142

For HD 169142 we find  $T_{\text{eff}} = 7500 \pm 200$  K, which is consistent with Guimarães et al. (2006), and  $\log g = 4.3 \pm 0.2$ , which is  $2\sigma$  greater than Guimarães et al. (2006) who find  $\log g = 3.7 \pm 0.1$ . If we were to adopt the  $\log g$  of Guimarães et al. (2006), it would decrease our abundances by between  $\sim 0.05$  and  $\sim 0.2$  dex depending on the element, which is generally within our uncertainties. We find a clear  $\lambda$  Boo pattern of abundances in this star. C and O are solar, and S is only slightly underabundant, while iron peak elements are underabundant by between 0.5 and 1 dex. Interestingly Ba and Nd are roughly solar, though Eu may be underabundant.

Alecian et al. (2012a) do not detect a magnetic field in HD 169142, nor do Hubrig et al. (2009).

#### A12 HD 176386

We derive an  $T_{\text{eff}}$  of  $11000 \pm 400$  K and a  $\log g$  of  $4.1 \pm 0.3$  for HD 176386. The abundances we derive for the star are consistent with solar, with the possible exception of Ca. Thus we conclude that the star is chemically normal.

No magnetic field was found for HD 176386 by Alecian et al. (2012a). Hubrig et al. (2009) claim a marginal detection at  $3\sigma$  in one observation. Bagnulo et al. (2011) re-reduced this observation and found no magnetic field. Thus, based on the majority of the evidence, we consider HD 176386 to be a non-magnetic star.

#### A13 HD 179218

For HD 179218 we derived  $T_{\text{eff}} = 9640 \pm 250$  K and  $\log g = 3.9 \pm 0.2$ , both of which are consistent with Guimarães et al. (2006). We find a solar He abundance, abundances of C, O, and Na that are marginally enhanced relative to solar, and N and S abundances that are uncertain, but apparently enhanced relative to solar. Iron peak elements are depleted relative to solar by  $\sim 0.5$  dex. We conclude that HD 179218 displays  $\lambda$  Boo peculiarities. The overabundances of C, N, O, and S may reflect an above solar intrinsic metallicity in the star, which the  $\lambda$  Boo peculiarities are superimposed upon. However, this is not certain, as He appears to have a nearly solar abundance.

Alecian et al. (2012a) find no magnetic field in HD 179218, which is supported by the non-detection of Hubrig et al. (2009).

#### A14 HD 244604

We found  $T_{\text{eff}} = 8700 \pm 220$  K and  $\log g = 4.0 \pm 0.2$  for HD 244604, which is consistent with the parameters from Acke & Waelkens (2004). We find most elements have solar abundances or are enhanced by around  $1\sigma$ . There is no evidence for selective depletion or enhancement. We conclude that the star is chemically normal. Acke & Waelkens (2004) were only able to determine an iron abundance for HD 244604,

though it is consistent with our abundance if we assume their uncertainty is similar to ours.

No magnetic field in HD 244604 is found by Alecian et al. (2012a). Wade et al. (2007) also find no magnetic field in the star, thus we consider the star to be non-magnetic.

#### A15 HD 245185

For HD 245185 we derive  $T_{\text{eff}} = 9500 \pm 750$  K and  $\log g = 4.0 \pm 0.4$ , which is consistent with Acke & Waelkens (2004). We find He, C, N, and O abundances that are consistent with solar, and iron peak abundances that are  $\sim 0.8$  dex below solar. While the uncertainties are relatively large for this star, the strong iron peak underabundances indicate  $\lambda$  Boo peculiarities. Acke & Waelkens (2004) were unable to determine any abundances for this star due to a low S/N in their observation and the high  $v \sin i$  of the star.

Alecian et al. (2012a) do not detect a magnetic field in the star, nor do Wade et al. (2007). Consequently, we consider the star to be non-magnetic.

#### A16 HD 278937 (IP Per)

For HD 278937 (IP Per) we find  $T_{\text{eff}} = 8000 \pm 250$  K and  $\log g = 4.1 \pm 0.2$ , which is consistent with the  $T_{\text{eff}}$  of Miroshnichenko et al. (2001), though they derive a  $\log g$  of  $4.4 \pm 0.1$  which is  $1\sigma$  above our value. The star is a known  $\delta$  Scuti pulsator (Ripepi et al. 2006). We find solar abundances for C, N, O, and S, while iron peak elements as well as Na, Mg, and Si are between 0.5 and 0.7 dex underabundant. This star shows clear  $\lambda$  Boo peculiarities. Miroshnichenko et al. (2001) found that HD 278937 had a metallicity below solar ( $[M/H] = -0.4$ ), based on a fit to the star's metallic line spectrum. This value is most likely a result of the low iron peak abundances in the star, and thus consistent with our abundances. The solar abundances of C, N, O and S were likely overlooked by the scaled solar abundance model of Miroshnichenko et al. (2001) due to the relative scarcity of lines of those elements. Therefore, the star is not a low metallicity star, but rather appears to have peculiar photospheric abundances.

No magnetic field is found in HD 278937 by Alecian et al. (2012a), or by Wade et al. (2007).

#### A17 T Ori

We find  $T_{\text{eff}} = 8500 \pm 300$  K and  $\log g = 4.2 \pm 0.3$  for T Ori. The abundances for He, C, N, and O are all consistent with solar, while the S abundance is almost  $3\sigma$  above solar. The S abundance is based only on two weak lines at 6749 and 6757 Å, and thus may be somewhat more uncertain than the error bar suggests. The iron peak abundances are clearly  $\sim 0.5$  dex below solar. We conclude that T Ori has clear  $\lambda$  Boo peculiarities

Neither Alecian et al. (2012a) nor Wade et al. (2007) detect a magnetic field in T Ori.

## Magnetic stars

### A18 HD 101412

HD 101412 was observed by Wade et al. (2005) and reanalysed by Wade et al. (2007) who found a longitudinal magnetic field of  $500 \pm 100$  G. The presence of a magnetic field was recently confirmed by Hubrig et al. (2009, 2011), and Alecian et al. (in prep.). Cowley et al. (2010) derived chemical abundances for HD 101412, and surprisingly discovered it had  $\lambda$  Boötis peculiarities. In our abundance analysis we find underabundances of iron peak elements, and solar C, O, and He, with values that are consistent with those of Cowley et al. (2010). Thus we confirm that HD 101412 has  $\lambda$  Boo peculiarities. While in main sequence A and B stars magnetic fields are associated with Ap and Bp chemical peculiarities, that is not the case for HD 101412.

We confirm the presence of an “anomalous saturation” in the lines of HD 101412 noted by Cowley et al. (2010). Even with a microturbulence of  $0 \text{ km s}^{-1}$ , when we fit weaker lines, stronger lines in the synthetic spectrum are often too deep to fit the observation. This problem is not consistent across all lines, and often appears to be fairly minor. This anomalous saturation does not appear to be common among HAeBe stars, as this is the only object for which we have seen this problem. A possible explanation for the discrepancy between the observations and the synthetic spectra is the presence of chemical stratification in the stellar atmosphere. Since stronger lines are often formed higher in the stellar atmosphere, if the abundance of some elements was lower higher in the atmosphere that would explain the apparent weakness of many stronger lines. The possibility of stratification will be investigated in detail in a future paper. The presence of veiling in the spectrum of this star would produce a similar discrepancy to what we see, however veiling would affect all lines of the same strength similarly, unlike the non-uniform trend we see. Thus we conclude veiling is unlikely to be the source of this discrepancy, in agreement with Cowley et al. (2010). The discrepancy is not likely to be a direct effect of the star’s magnetic field on line formation, which usually desaturates lines, and we do not find the problem in the other magnetic stars of our sample.

Placing HD 101412 on the H-R diagram, we find it has an age of  $1.2^{+0.8}_{-0.7}$  Myr and a mass of  $3.0 \pm 0.3 M_{\odot}$ , both of which are consistent with Wade et al. (2007). Since the star has no Hipparcos parallax, we adopted the distance of 500-700 pc proposed by Vieira et al. (2003), however this is somewhat uncertain. Even with this uncertainty, the star falls well before the beginning of the main sequence on the H-R diagram, thus the star is almost certainly a pre-main sequence object.

We find similar  $\lambda$  Boo type peculiarities in many of the non-magnetic HAeBe stars in our sample, thus this feature is not unique to HD 101412, or to magnetic HAeBe stars. Indeed, it appears that the peculiarities in HD 101412 occur in a significant fraction of all HAeBe stars.

### A19 HD 190073

HD 190073 has a magnetic field, discovered and repeatedly detected by Catala et al. (2007), with a longitudinal strength of  $74 \pm 10$  G that was constant over the course of their observations. In our analysis we find that the star is chemically

normal, as shown in Fig. A5. Apparent over abundances relative to solar in N and Na may be due to non-LTE effects, or weak undiagnosed blends, since for both elements only a couple of very weak lines were usable for our analysis.

Acke & Waelkens (2004) analysed HD 190073 and adopted  $T_{\text{eff}} = 9250$  K and  $\log g = 3.5$ , which is consistent with our values of  $T_{\text{eff}} = 9230 \pm 260$  K and  $\log g = 3.7 \pm 0.3$ . Based on equivalent widths, they found abundances for C, N, O, Mg, Si, Ca, Sc, Ti, V, Cr, Fe, Ni, Y, Zr, and Ba, all of which are consistent with ours. For Al they found an abundance  $-0.45$  dex below solar, based on only one line, which is inconsistent with our value. Our abundance is based on two lines, thus we consider it to be the more accurate value. Our result leads to a nearly solar abundance, consistent with other elements in this star.

We find that the star is quite young ( $1.6 \pm 0.6$  Myr), which agrees with the age determined by Catala et al. (2007) of  $1.2 \pm 0.6$  Myr. Thus it is possible that the star has not yet had time to build up significant chemical peculiarities on its surface. This hypothesis is supported by the modelling of Vick et al. (2011), who found that it takes at least  $\sim 2$  Myr for a  $2.9 M_{\odot}$  star to develop significant chemical peculiarities by radiative diffusion.

### A20 V380 Ori A & B

V380 Ori is a triple star system, with two components detectable spectroscopically (Alecian et al. 2009). The more massive spectroscopic component (the primary) shows no detectable change in radial velocity, while the fainter, less massive (secondary) component’s radial velocity varies with a period of  $\sim 100$  days (Alecian et al. 2009). The third component in the system was detected by speckle interferometry in the infra red (Leinert et al. 1997), but is not detectable in the visible spectrum of the system (Alecian et al. 2009). The primary has a magnetic field, detected by Wade et al. (2005), while the secondary has no detectable magnetic field. The magnetic field of the primary was repeatedly observed by Alecian et al. (2009), who modelled the geometry as a dipole, with a strength of  $2120 \pm 150$  G, and an obliquity of  $66 \pm 5^{\circ}$ .

Modelling the spectrum of the V380 Ori system was done somewhat differently than for the other stars in this study. Spectral disentangling was inapplicable due to the large amounts of variable emission in the spectrum, and the lack of radial velocity variation in the primary. Instead we fit a composite synthetic spectrum directly to the observation. The composite spectrum was constructed by adding the synthetic spectra of both stars, in absolute flux, weighted by the squared ratio of radii of the stars (the  $T_{\text{eff}}^4$  dependence is included in the absolute fluxes of the synthetic spectra). The combined spectrum was then normalised by the sum of the continuum fluxes, also weighted by the ratio of radii squared. Using this composite spectrum, the model parameters for one star were simultaneously fit by  $\chi^2$  minimisation, while the other star’s parameters were held fixed. The ratio of radii was simultaneously fit as well, but the radial velocities of the two components were determined before the rest of the fitting process. The combination of parameters for both stars from one spectral window was determined iteratively, alternating between the two stars, and fitting the parame-

ters of one while holding the parameters of the other fixed. Initial parameters were taken from Alecian et al. (2009).

We find chemical peculiarities in the primary that are consistent with Ap/Bp peculiarities. The peculiarities are weak, but detectable. C, S, and Ne are within uncertainty of solar, while Fe, Ni, and Mn are overabundant by more than  $3\sigma$ . Si is also overabundant by more than  $4\sigma$  in the primary, and He may be overabundant at  $2.2\sigma$ . The abundances of the secondary are uncertain, but consistent with solar. Most elements in the secondary are within  $1\sigma$  of solar, and all elements are within  $2\sigma$  (except for Ba). The large uncertainty in the secondary stems mostly from the uncertainty in the ratio of radii (and hence ratio of luminosities) for the system, though uncertainties in effective temperature also play a role. While the average abundance in the secondary appears to be slightly above solar, it is not clear whether this reflects an intrinsically higher metallicity in the system, or if the luminosity ratio has simply been slightly overestimated. The abundances derived for the secondary are highly sensitive to the adopted ratio of radii, however the abundances for the primary are not, since the primary dominates the luminosity of the system.

We find a ratio of radii for the V380 Ori system of  $R_A/R_B = 0.7 \pm 0.1$ . The relatively large radius of the secondary is a consequence of the star being less massive, and thus being slower to contract towards the main sequence than the more massive primary. The H-R diagram positions of the two stars are consistent with a single isochrone.

The appearance of chemical peculiarities in the primary of V380 Ori is consistent with the modelling by Vick et al. (2011), who discuss this system in some detail. Since the primary is more evolved than HD 190073, it could have developed chemical peculiarities while HD 190073 has not yet.

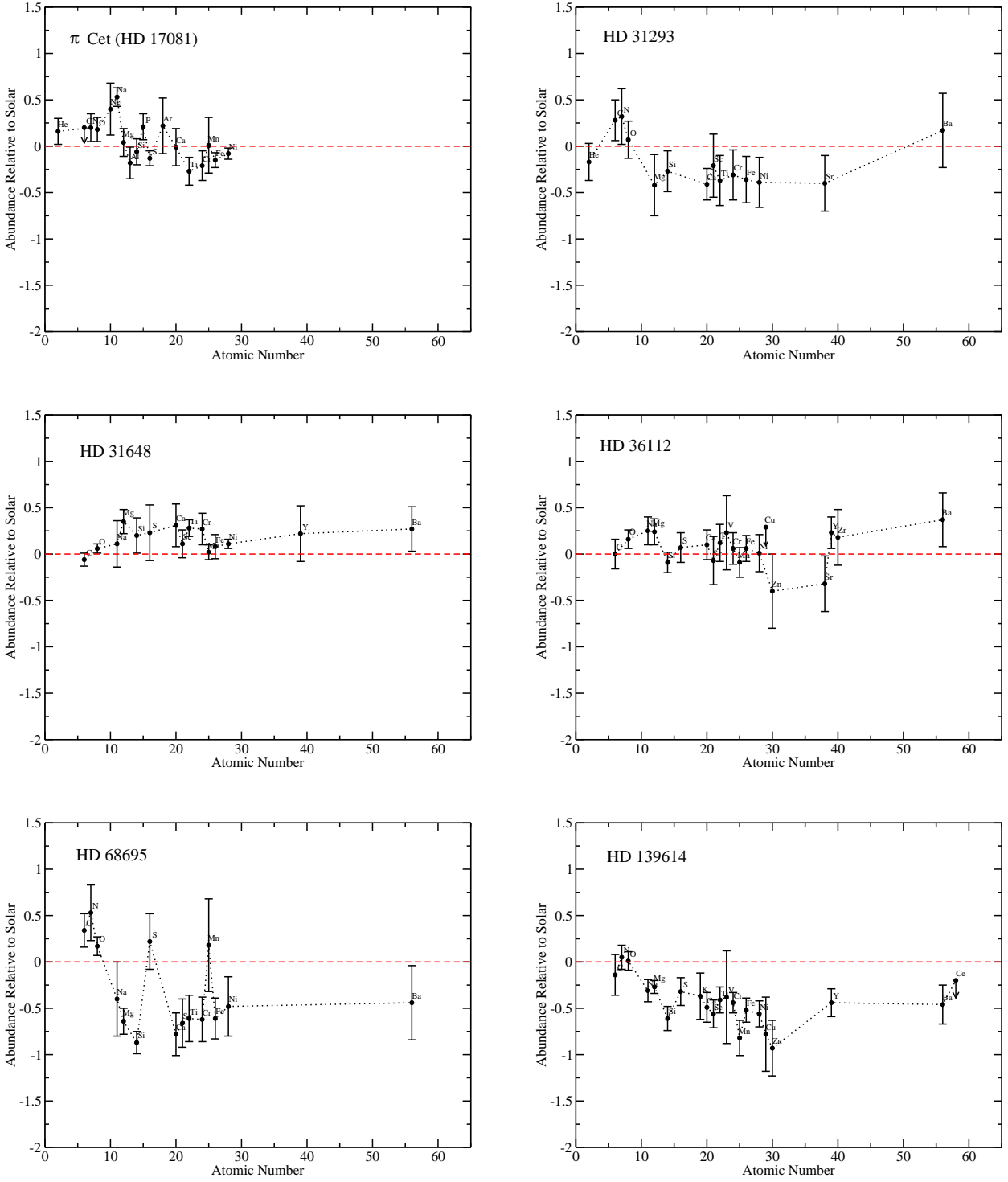


**Figure A2.** Final abundances relative to solar for the stars in this study. Solar abundances are taken from Grevesse et al. (2005). Points marked with an arrow represent upper limits only.

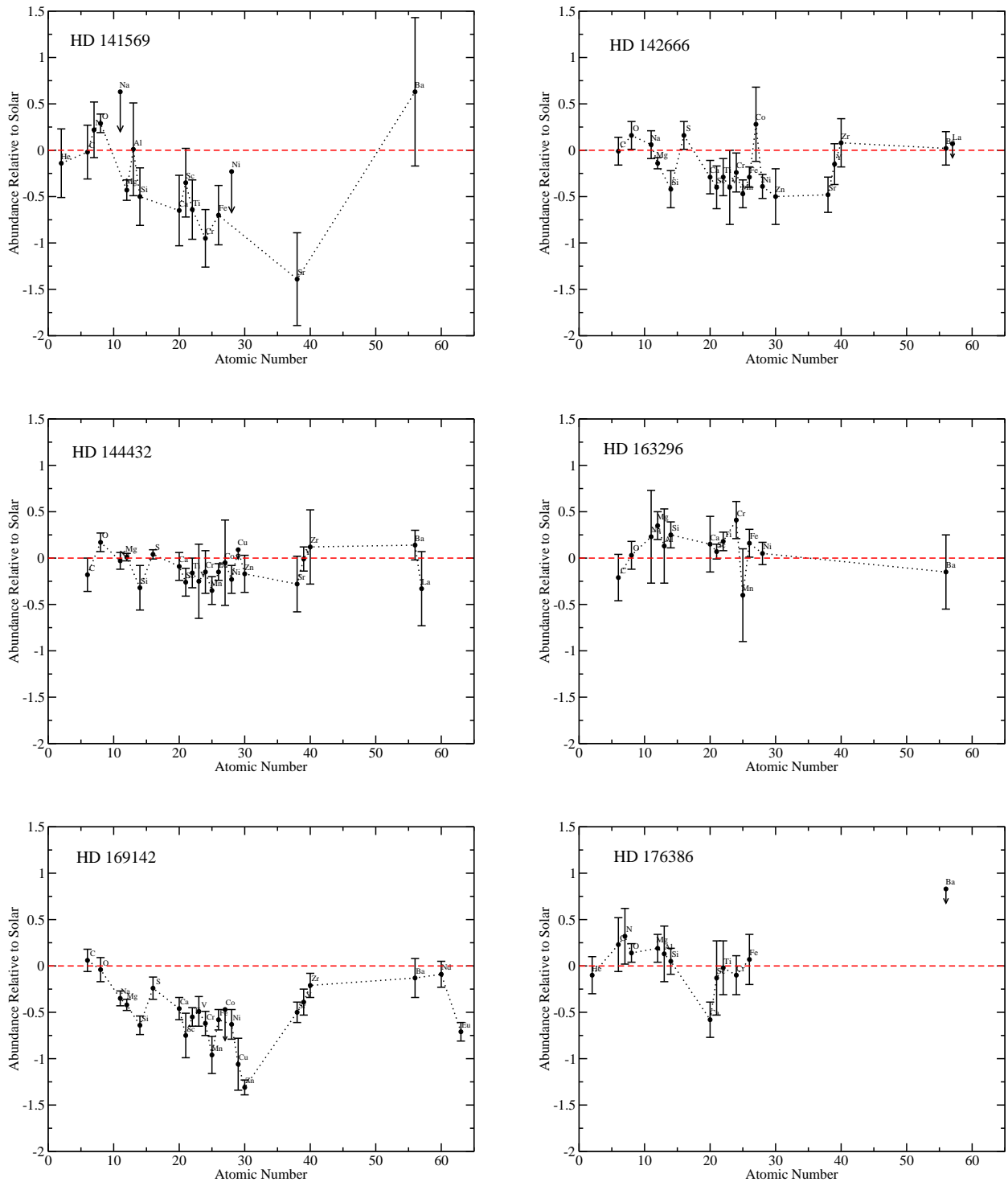


**Figure A3.** Final abundances relative to solar for the stars in this study, as in Fig. A2.

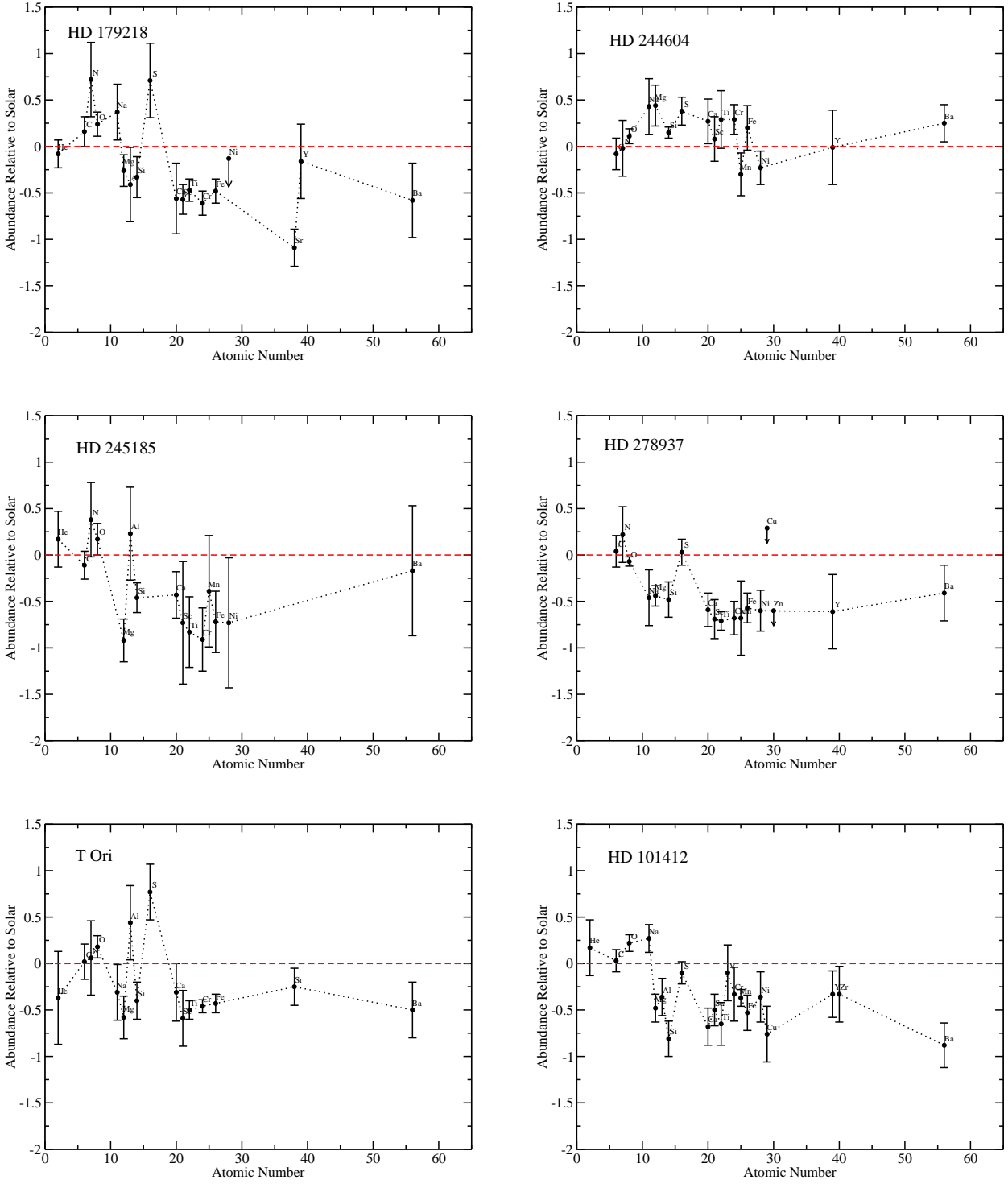
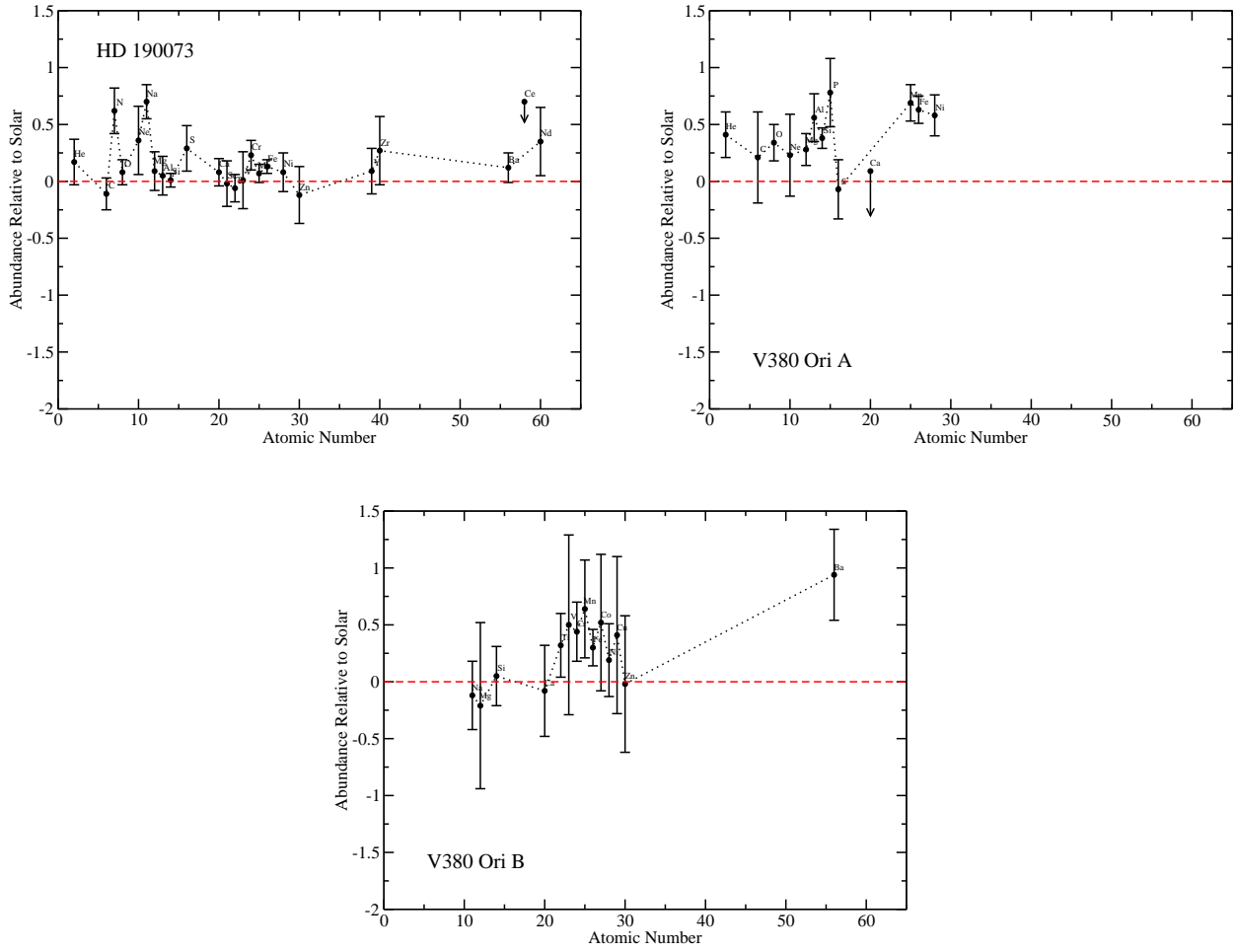
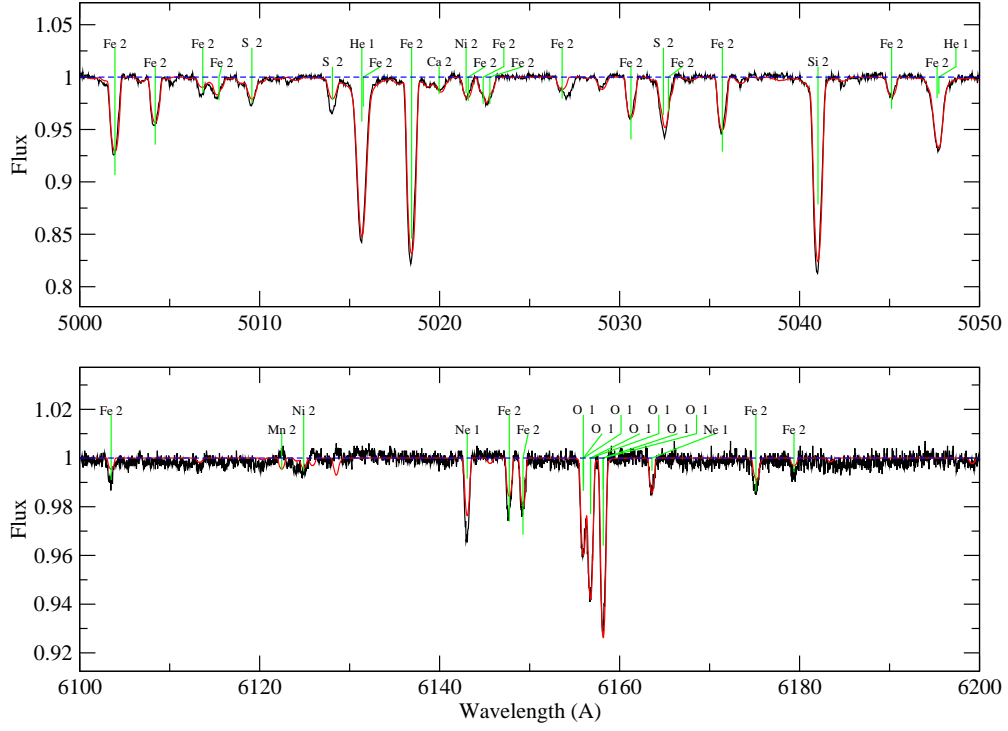


Figure A4. Final abundances relative to solar for the stars in this study, as in Fig. A2.



**Figure A5.** Final abundances relative to solar for the stars in this study, as in Fig. A2.



**Figure A6.** Comparison of the observed spectrum (jagged line) to the best fit synthetic spectrum (smooth line) for  $\pi$  Cet (HD 17081). Two independent wavelength regions are presented. Lines have been labelled by their major contributing species. Gaps in the synthetic spectra indicate regions that were not fit.

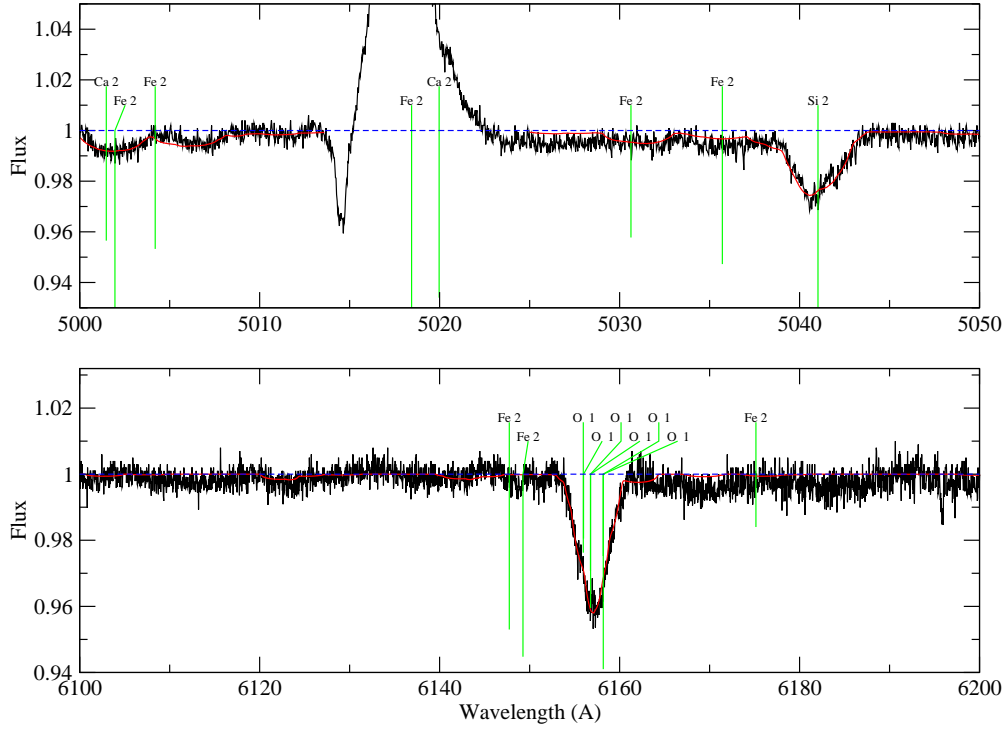


**Figure A7.** Comparison of the observed spectrum to the best fit synthetic spectrum for HD 31293, as in Fig. A6

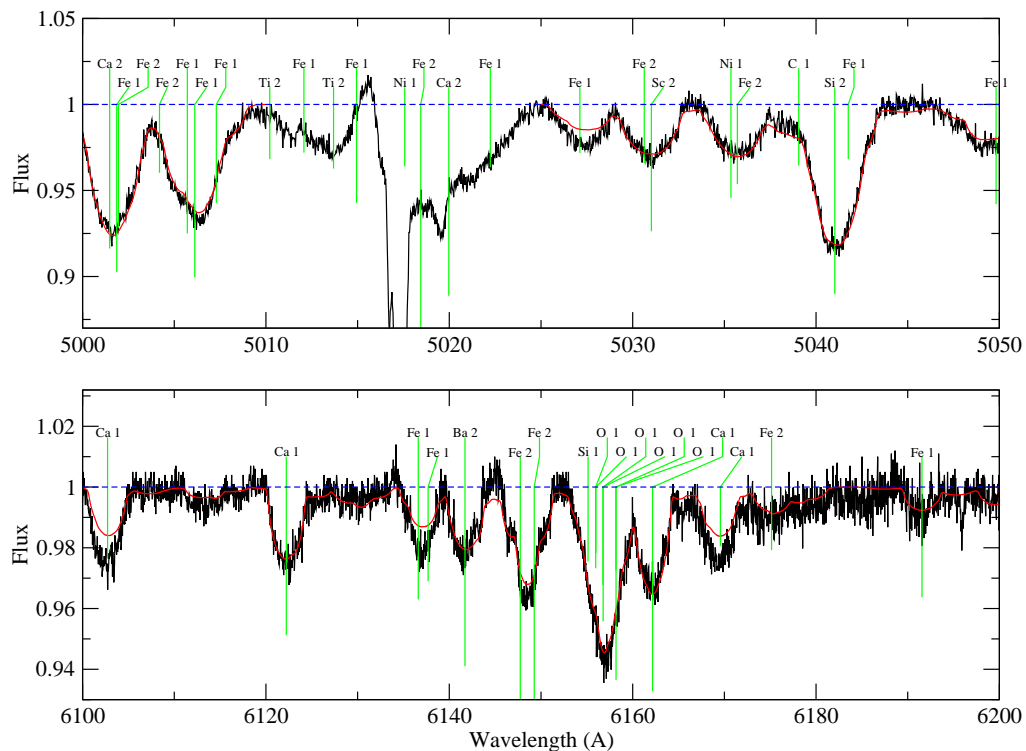


**Figure A8.** Comparison of the observed spectrum to the best fit synthetic spectrum for HD 31648, as in Fig. A6

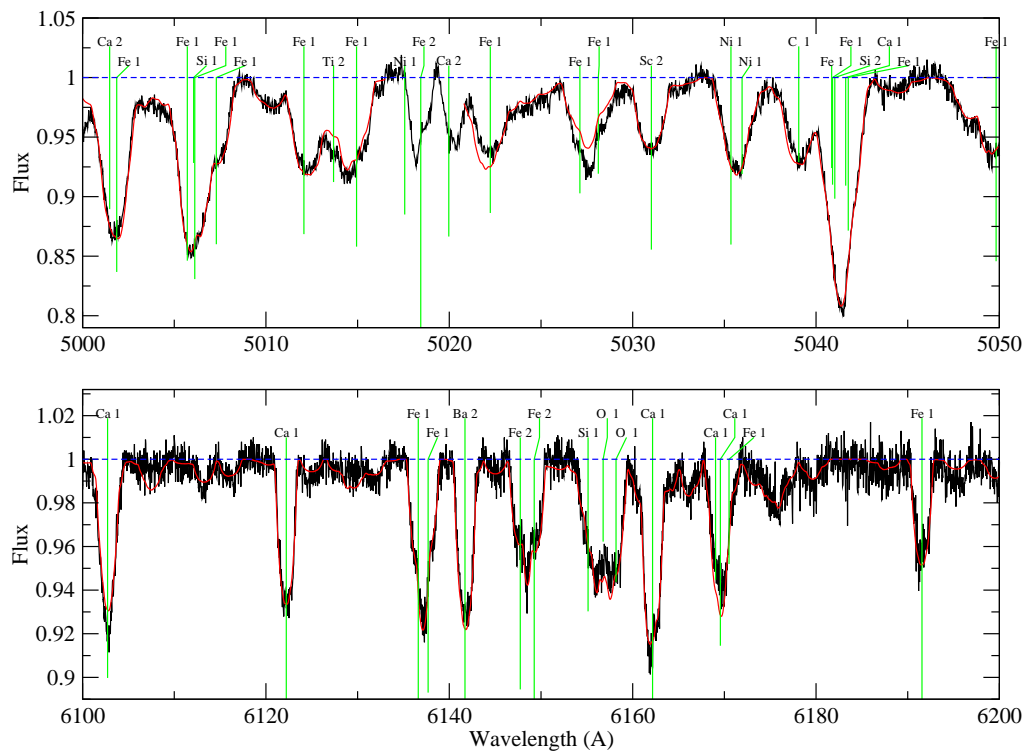


**Figure A9.** Comparison of the observed spectrum to the best fit synthetic spectrum for HD 36112, as in Fig. A6

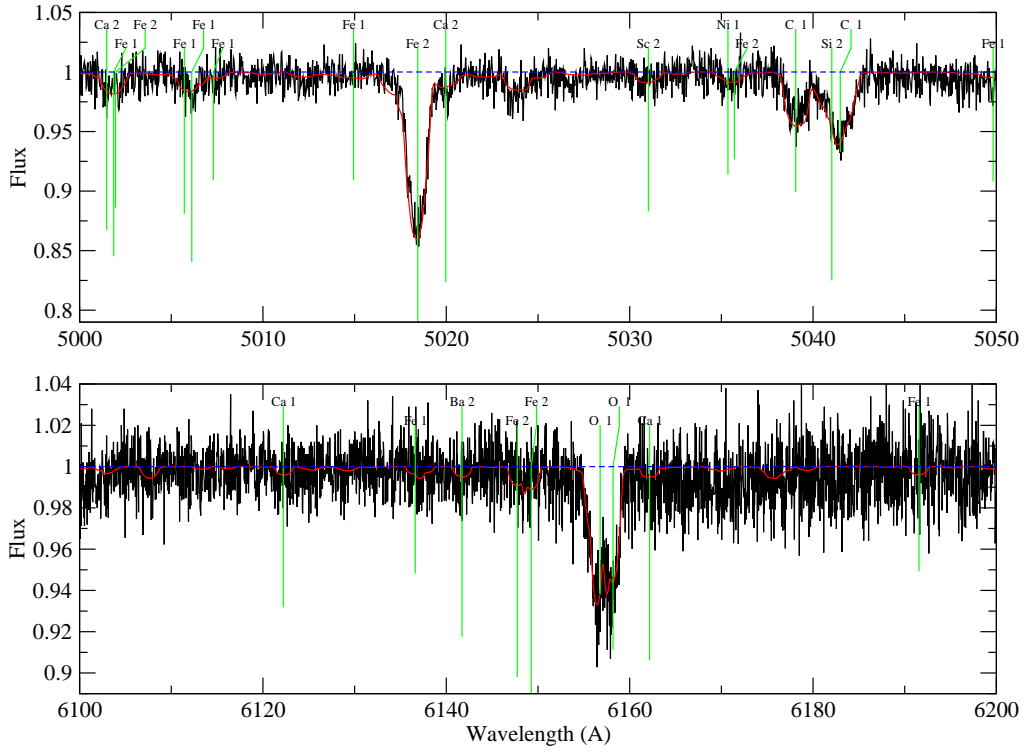


Figure A10. Comparison of the observed spectrum to the best fit synthetic spectrum for HD 68695, as in Fig. A6

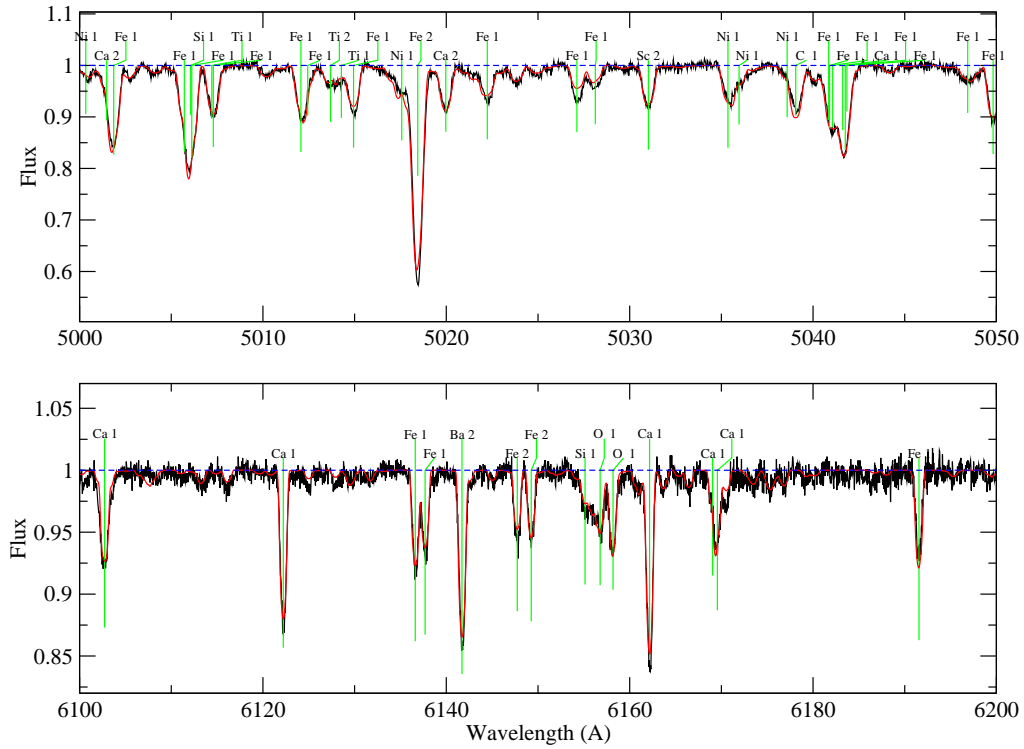
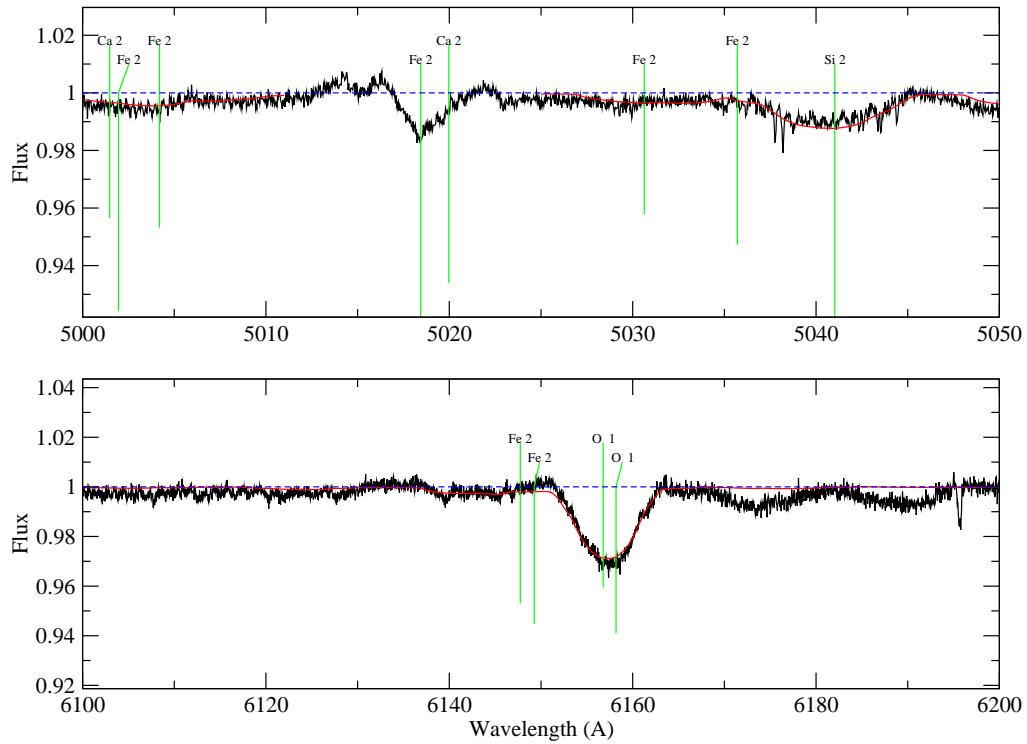
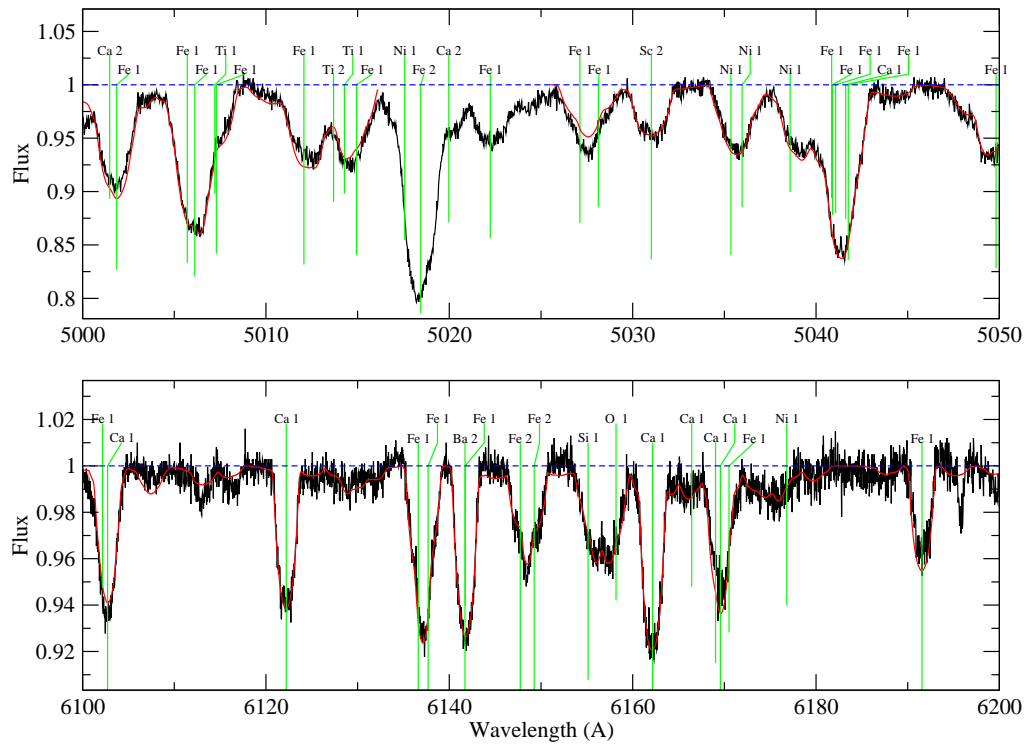


Figure A11. Comparison of the observed spectrum to the best fit synthetic spectrum for HD 139614, as in Fig. A6



**Figure A12.** Comparison of the observed spectrum to the best fit synthetic spectrum for HD 141569, as in Fig. A6



**Figure A13.** Comparison of the observed spectrum to the best fit synthetic spectrum for HD 142666, as in Fig. A6

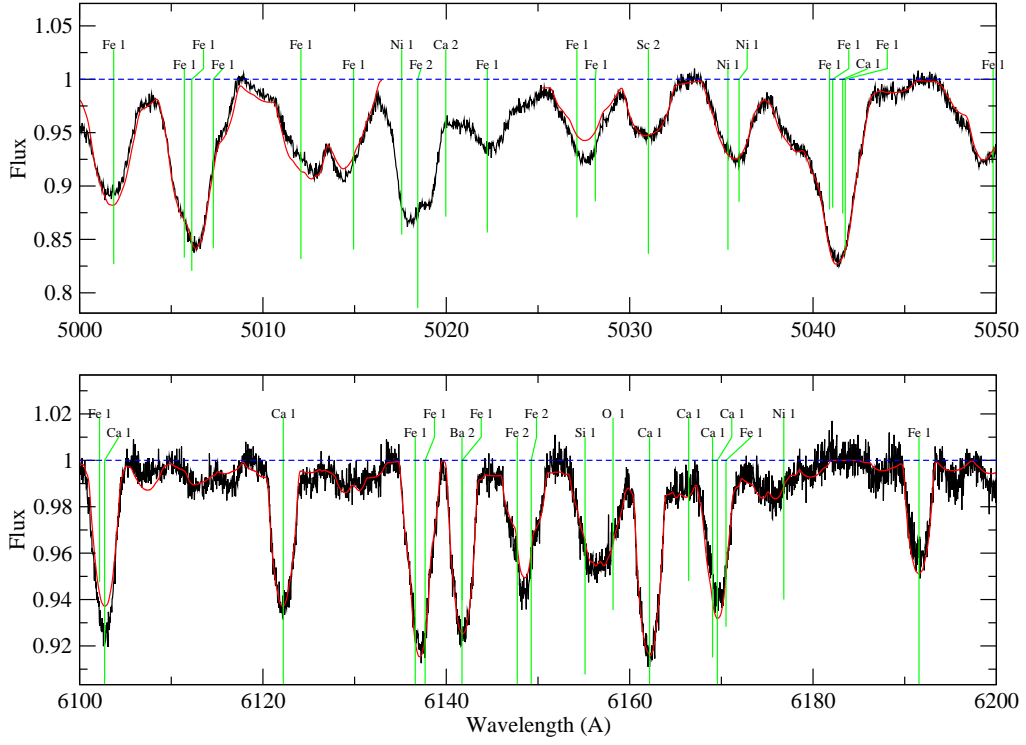


Figure A14. Comparison of the observed spectrum to the best fit synthetic spectrum for HD 144432, as in Fig. A6

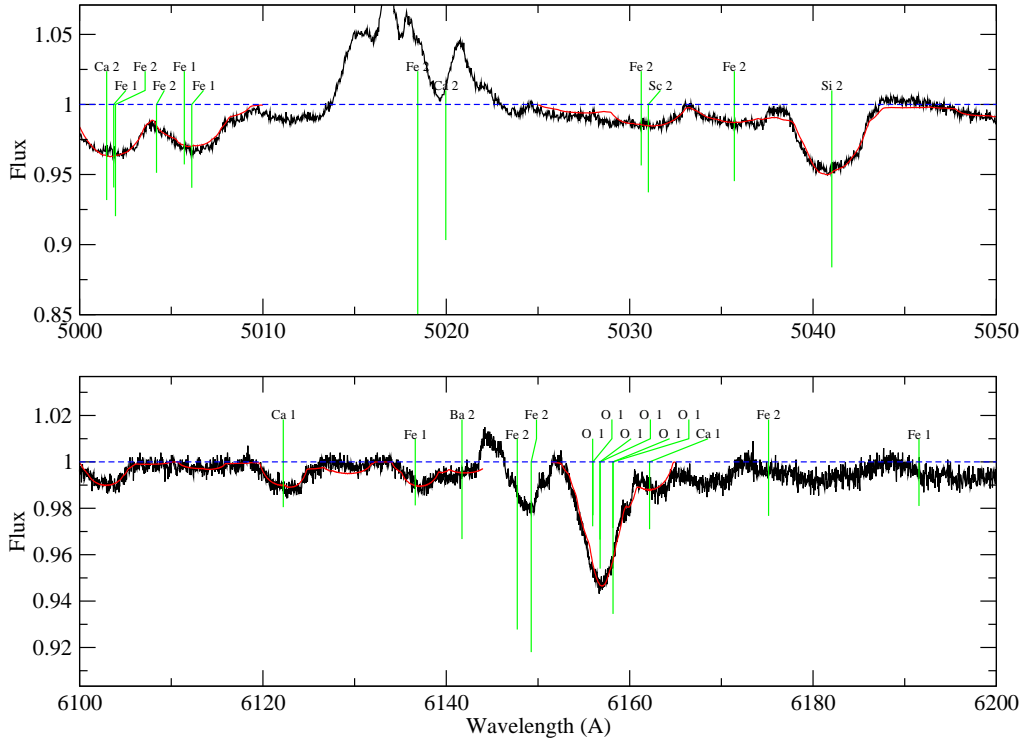


Figure A15. Comparison of the observed spectrum to the best fit synthetic spectrum for HD 163296, as in Fig. A6



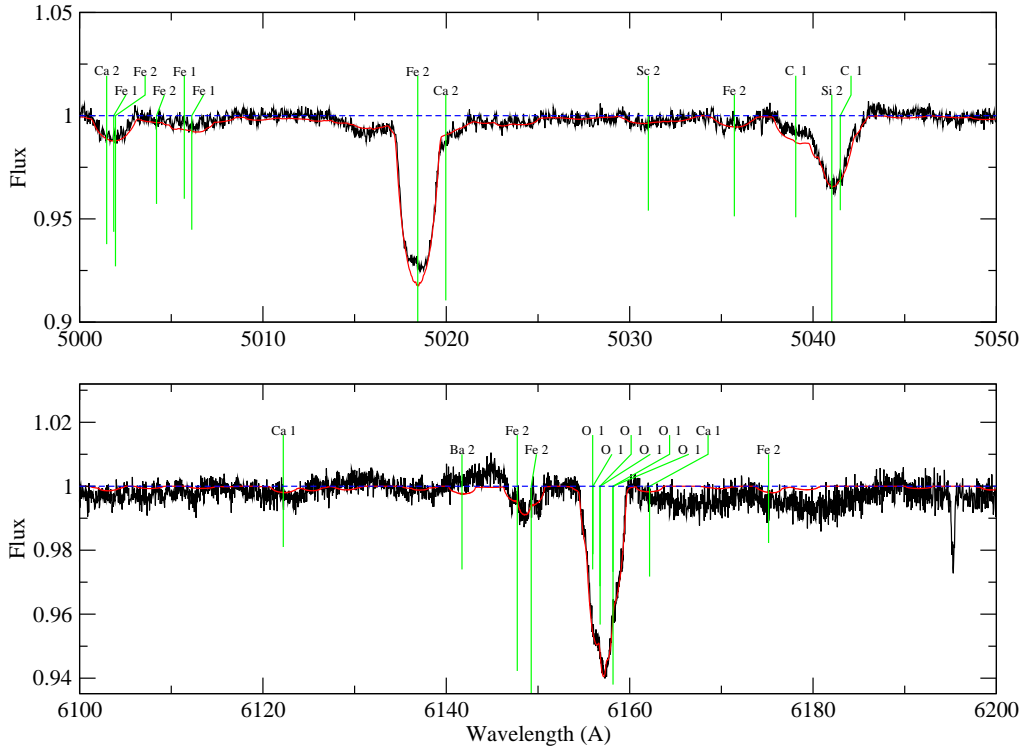


Figure A18. Comparison of the observed spectrum to the best fit synthetic spectrum for HD 179218, as in Fig. A6

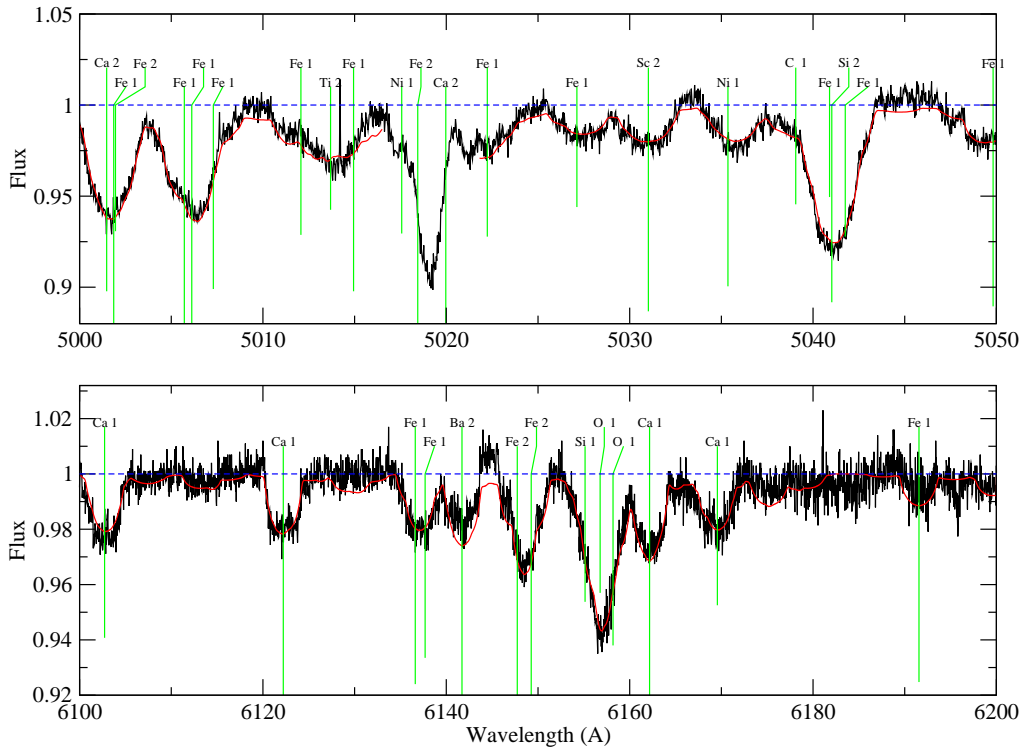
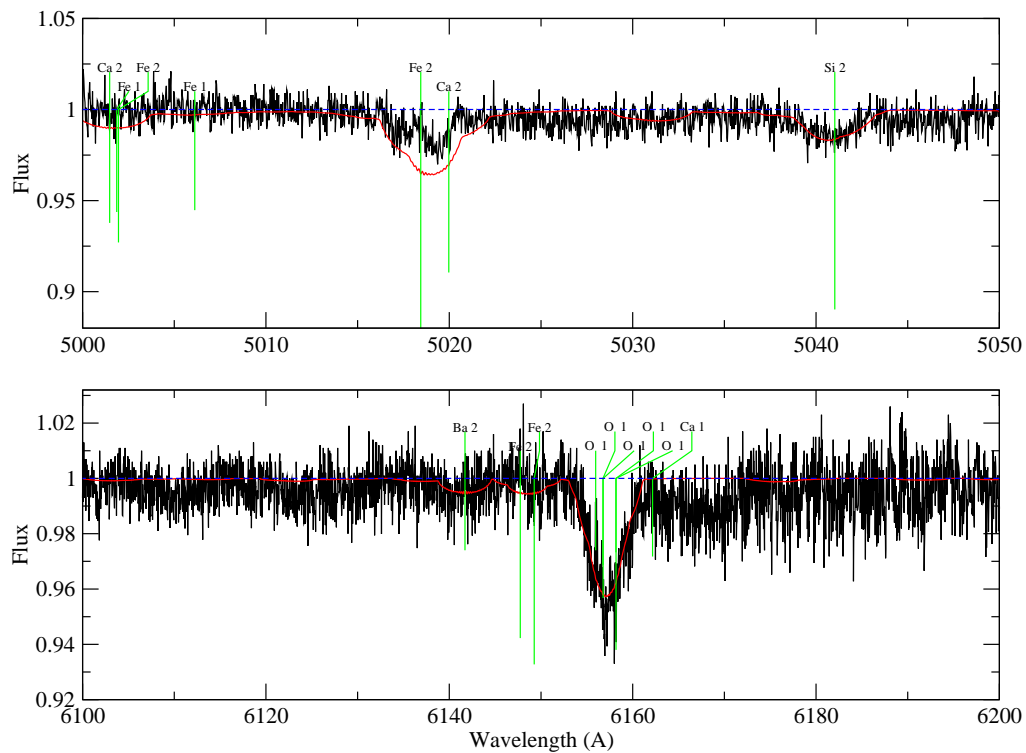
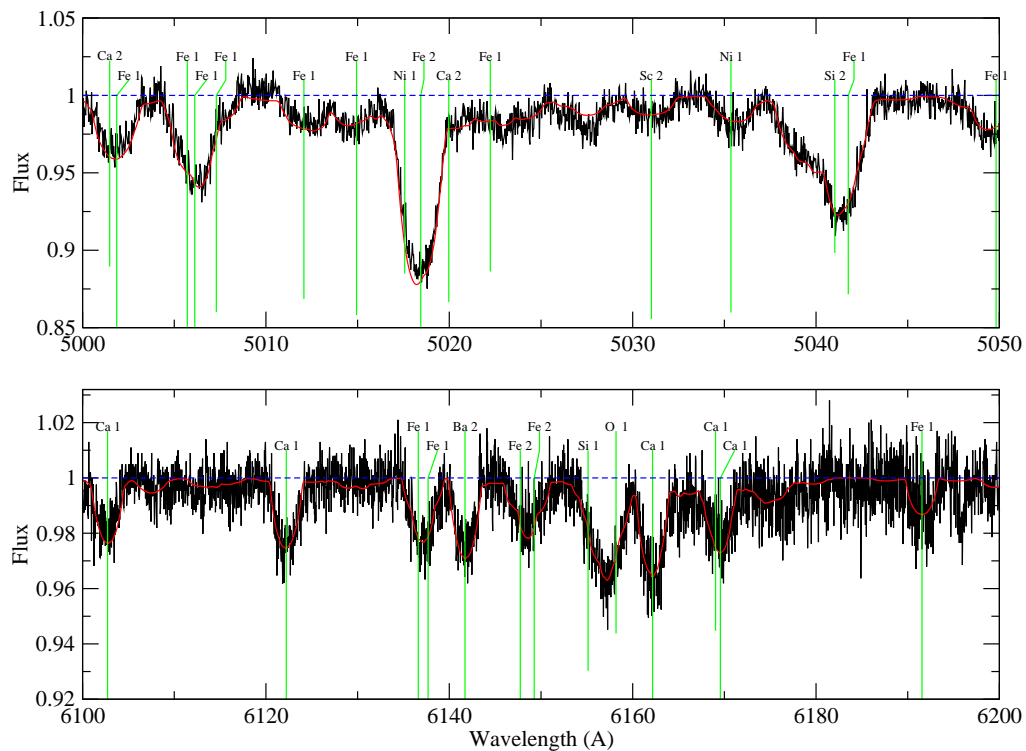


Figure A19. Comparison of the observed spectrum to the best fit synthetic spectrum for HD 244604, as in Fig. A6



**Figure A20.** Comparison of the observed spectrum to the best fit synthetic spectrum for HD 245185, as in Fig. A6



**Figure A21.** Comparison of the observed spectrum to the best fit synthetic spectrum for HD 278937, as in Fig. A6

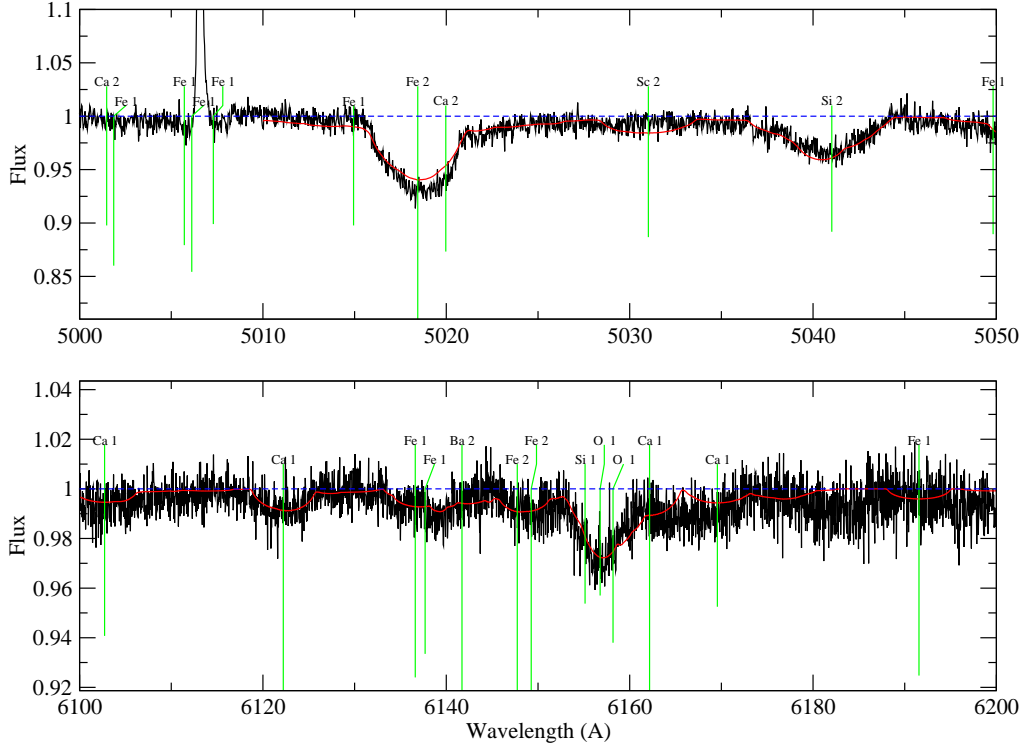


Figure A22. Comparison of the observed spectrum to the best fit synthetic spectrum for T Ori, as in Fig. A6

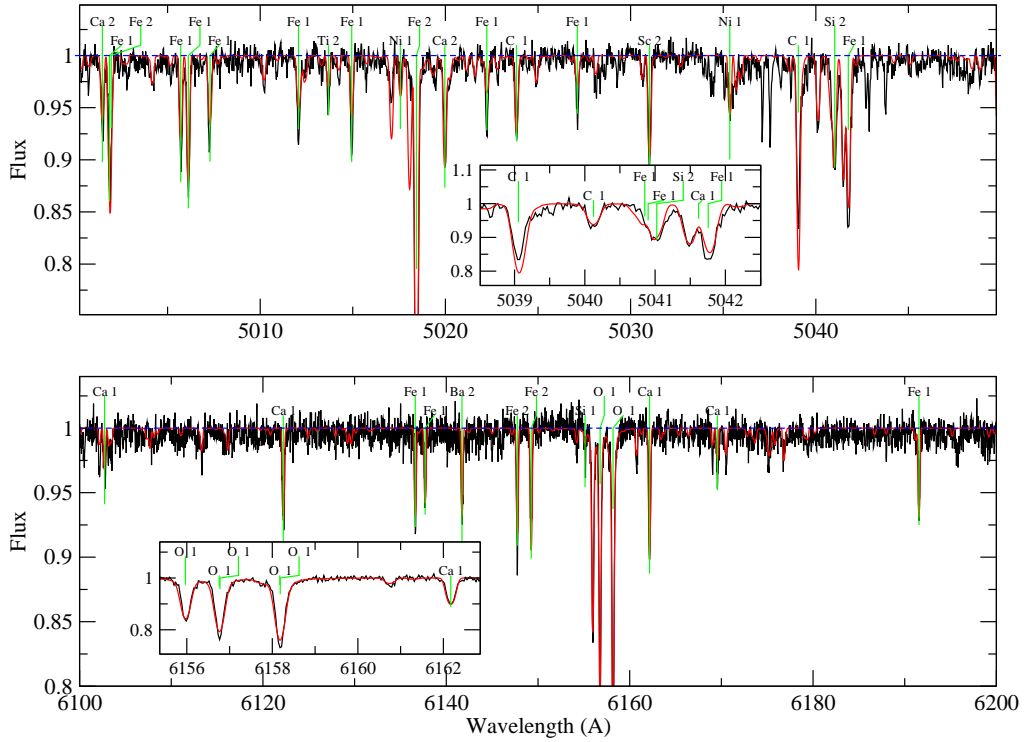
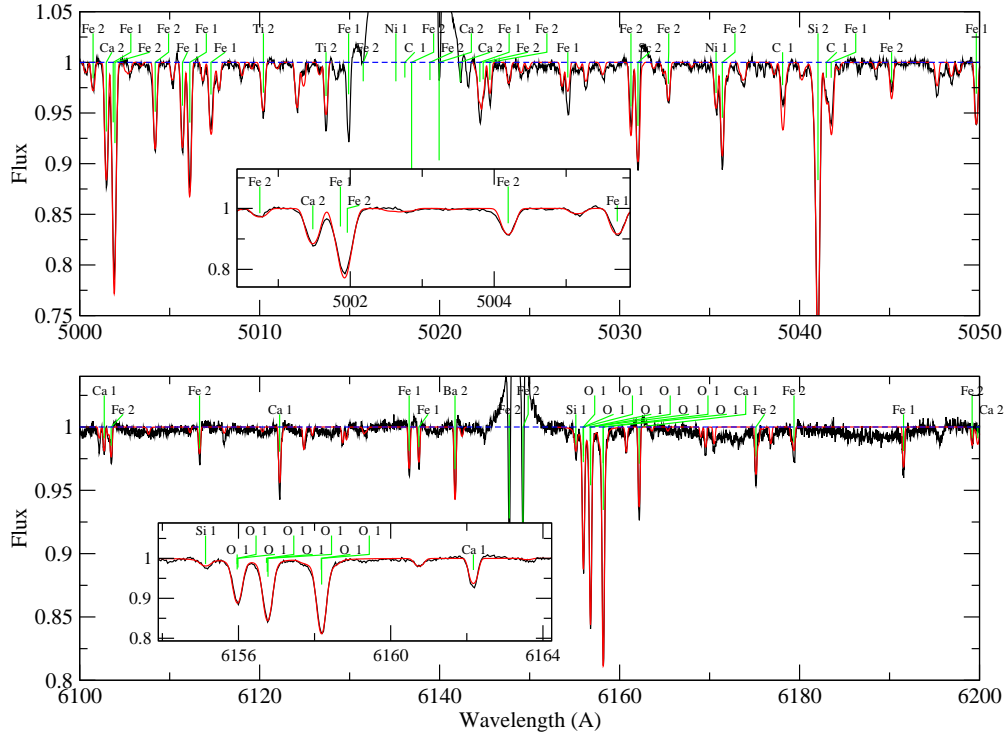
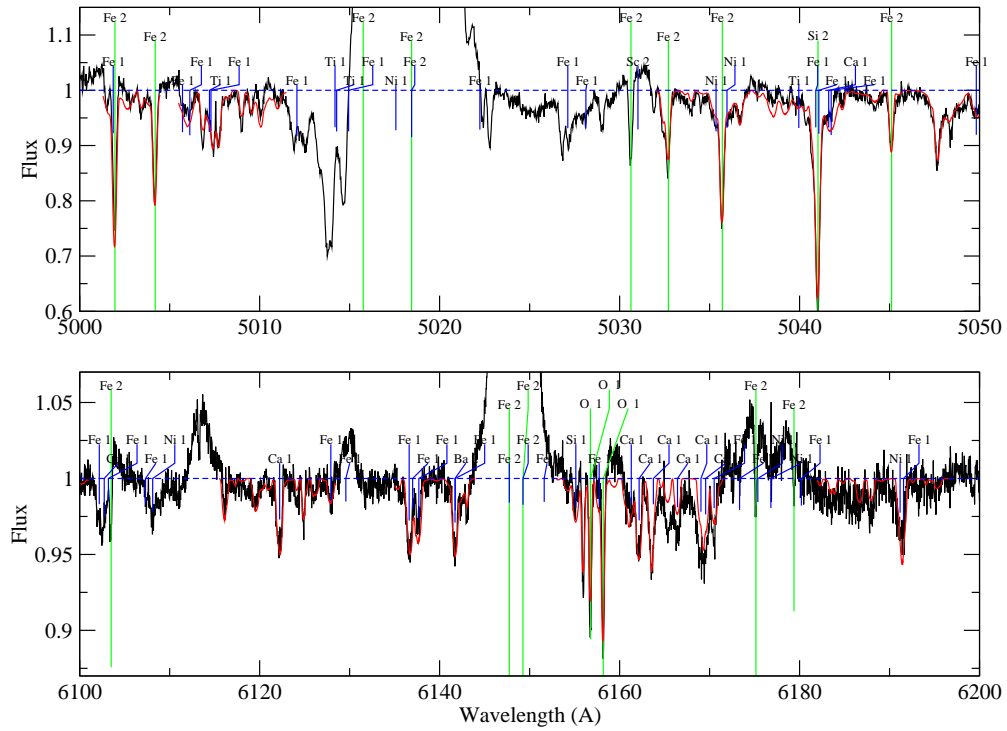


Figure A23. Comparison of the observed spectrum to the best fit synthetic spectrum for HD 101412, as in Fig. A6



**Figure A24.** Comparison of the observed spectrum to the best fit synthetic spectrum for HD 190073, as in Fig. A6



**Figure A25.** Comparison of the observed spectrum (jagged line) to the best fit synthetic spectrum of the combined V380 Ori A and B system (smooth line). The upper two rows of line labels (green) indicate lines of the primary, the lower two rows (blue) indicate lines of the secondary. Gaps in the synthetic spectrum indicate regions that were excluded from the fit.

This paper has been typeset from a  $\text{\TeX}$ / $\text{\LaTeX}$  file prepared by the author.